Characteristics for the Occurrence of a High-Current Z-Pinch Aurora as Recorded in Antiquity Part II: Directionality and Source

Anthony L. Peratt, *Fellow, IEEE*, John McGovern, Alfred H. Qöyawayma, *Life Member, IEEE*, Marinus Anthony Van der Sluijs, and Mathias G. Peratt, *Member, IEEE*

***Abstract*—The discovery that objects from the Neolithic or Early Bronze Age carry patterns associated with high-current Z-pinches provides a possible insight into the origin and meaning of these ancient symbols produced by humans. Part I deals with the comparison of graphical and radiation data from high-current Z-pinches to petroglyphs, geoglyphs, and megaliths. Part I focused primarily, but not exclusively, on petroglyphs of some 84 different morphologies: pictures found in laboratory experiments and carved on rock. These corresponded to mankind's visual observations of ancient aurora as might be produced if the solar wind had increased (T. Gold) at times between one and two orders of magnitude, millennia ago. Part II focuses on the source of light and its temporal change from a current-increasing Z-pinch or dense-plasma-focus aurora. Orientation and field-of-view data are given as surveyed and contributed from 139 countries, from sites and fields containing several millions of these objects. This information allows a reconstruction of the auroral form presumably associated with extreme geomagnetic storms and shows, based on existent geophysical evidence, plasma flow inward at Earth's south polar axis.**

***Index Terms*—Archaeoastronomy, aurora, dense plasma focus (DPF), global information systems, magnetohydrodynamic (MHD) instability, petroglyph, plasma, plasma universe, Z-pinch.**

I. Introduction

THE DISCOVERY that objects from the Neolithic or Early Bronze Age carry patterns associated with high-current Z-pinches provides a possible insight into the origin and meaning of these ancient symbols produced by humans [1]–[3]. Part I, Characteristics for the Occurrence of a High-Current Z-pinch Aurora as Recorded in Antiquity [4], dealt with the comparison of graphical and radiation data from high-current Z-pinches to the images of petroglyphs, geoglyphs, and megaliths.

Part I focused primarily, but not exclusively, on petroglyphs of some 84 different morphologies: those found in laboratory experiments which are similar to those carved on rock. As the same morphological types are found worldwide, the comparisons suggest a type of single visible source. The striking similarity of petroglyphs to plasma experiments would indicate that they are reproductions or parts of reproductions of intense electrical phenomena, an obvious high-energy visible source that would be external to the Earth, such as the solar-wind aurora we observe today. However, laboratory experiments, when compared to ancient recordings, suggest the occurrence of an intense aurora, as might be produced if the solar wind had increased between one and two orders of magnitude, millennia ago.

A past intense solar outburst and its effect on Earth was proposed by Gold [5] who, along with others, based his hypotheses on strong astronomical and geophysical evidence.

According to Gold:

> "The question I would like to tackle is whether solar outbursts of the present day are representative of all that has happened in geologic times or whether much greater outbursts have occurred from time to time. Our evidence that nothing very violent has taken place in historic times is concerned with such a short span of time only that it cannot answer the question.
>
> For one big outburst every ten thousand years, for example, it would be permissible to have 2×10^{-5} of the present atmosphere removed every time. That means the outburst could be intense enough to drive down to the 20 μ bar level and blast away everything above that level. The change in atmospheric pressure resulting would only have minor climatic consequences.
>
> It is of interest to consider the magnetic storm effects such an outburst. The simple rule about the magnetic field strength generated at a large obstacle in the interplanetary stream is that the magnetic pressure will rise until it equals the stagnation pressure of the flow: $H^2/8\pi = \rho\nu^2$. The solar gas driving at the Earth will thus augment its field on compression, and for the intensity of the stream we were discussing where the stagnation pressure amounts to 20 dynes/cm^2 the field strength would be about 20 gauss.

Manuscript received February 20, 2007; revised June 3, 2007. This work was supported in part by the Mainwaring Archive Foundation and in part by the National Nuclear Security Agency, Washington, DC.

A. L. Peratt is with the Applied Physics Division, Los Alamos National Laboratory, Los Alamos, NM 87545 USA, and also with the University of Pennsylvania Museum of Archaeology and Anthropology, Philadelphia, PA 19104 USA (e-mail: alp@ieeetps.org; alp@lanl.gov).

J. McGovern is with the Institute for Epigraphic and Aboriginal Recordings, Georgetown, S.A. 5472, Australia.

A. H. Qöyawayma is with Qöyawayma Ceramics and Epigraphics, Prescott, AZ 86301 USA.

M. A. Van der Sluijs is with Mythopedia, London, U.K.

M. G. Peratt is with the Network Communications Systems, Raytheon Corporation, Fullerton, CA 92831 USA.

Color versions of one or more of the figures in this paper are available online at http://ieeexplore.ieee.org.

Digital Object Identifier 10.1109/TPS.2007.902630

> A magnetic storm of that kind of severity would be a totally different kind of phenomenon from the usual one. The Earth's magnetic field could clearly not hold up the incoming gas, and it would indeed drive down to the atmospheric level where the gas pressure can resist the further flow. At that level the atmosphere is dense and the ionization that could be maintained would not result in a good conductivity. The incoming gas bringing its strong fie1d into the virtually insulating atmosphere would then result in very large electric fields so directed that the resulting currents would maintain those fields. But in the atmosphere they can be done only by electrical breakdown. ... This breakdown would be in the form of a series of sparks, burning for extended periods of time and carrying currents of hundreds of millions of amperes. One might search whether there is any geological record of surface fusing and vitrification of rock or sand which cannot be accounted for by volcanic or meteoritec events. Large quantities of glass, far too much to be made by ordinary lightning discharges, are indeed found on the surface in a few places, notably in the Libyan Desert. Perhaps it might be worthwhile to pursue this clue further.
>
> ... One cannot at the present time make a case for occasional giant outbursts on the sun; but on the other hand, one must not ignore the possibility in the discussion of many lines of evidence in astronomy, geophysics and geology."

The answer to Gold's question seems to come from an unlikely source: Magnetized plasma from intense solar discharges striking the Earth's space environment as recorded by mankind in antiquity.

In Part I, direct comparison was made of some 40% of data carved on rock to that recorded in laboratories and in high-explosive high-energy tests with current magnitudes similar to that found in auroras today. The sources of these patterns were magnetohydrodynamic (MHD) instabilities from intense Birkeland currents, a Z-pinch, flowing to the Earth [6].

Other patterns could be attributed to and found to replicate Rayleigh–Taylor instabilities, as found experimentally and in computer simulations, when a relativistic-electron beam (REB) impacts the upper atmosphere [6]. The last category of petroglyphs depicting instability could be attributed to the diocotron or slip-stream instability associated with hollow REBs, which may produce some curtain patterns in contemporary auroras [7].

In Part II, Directionality and Source, we focus both on field data of logged petroglyphs and on sources of light and their temporal change from current-increasing Z-pinch aurora. Orientation and field-of-view (FOV) data from sites containing many millions of these objects in 139 countries are given as surveyed. This information allows a reconstruction of the auroral form and shows, for existent geophysical evidence, that relativistic electrons generated in such extreme geomagnetic storms primarily flow inward at Earth's south polar axis [8]–[16].

II. Methodology

This paper is the second of three parts. Part I dealt with the correspondence of petroglyph images worldwide to MHD instabilities. Some 84 different instability configurations were compared, petroglyph to plasma, providing temporal information for petroglyph symbols from laboratory recordings. The high-energy-density experiments and tests are close to what is expected when a giga-ampere current impinges on the Earth, allowing direct petroglyph–laboratory comparisons including computer-generated time–motion studies of evolution. Some 40% of known symbols were accounted for. The similarities and differences of petroglyphs and pictographs were also discussed in Part I.

Part III fills in the remainder of known symbols and relies heavily on what is present in Part II, this paper. Here, we analyze the orientation and distribution of petroglyphs around the Earth: where they are, where they are not, their directionality, FOV of the current column, and the inclination angle at which the artist was observing.

As such, this paper (Part II) goes into some detail about the recorded data, briefly summarizing satellite, aerial, and 3-D topographic data. The importance of this data cannot be over emphasized: Petroglyphs are treated as pixels; the FOVs and symbol orientations of any unmoved petroglyph allow the construction of a virtual image of the original aurora as if it were a hologram.

A. Data Acquisition

With the petroglyph–intense-aurora connection, it became important to GPS log as many individual petroglyphs as possible. Teams of interested archaeologists, students, retired university professors, and others were organized. Initially, a large team consisting of petroglyph-site stewards based in Tucson, Arizona, along with participants from New Mexico, started logging the Southwest.

A smaller team of some eight people began logging the Pacific Northwest, particularly the Columbia River Basin.

GPS receivers of all makes, surveyors' transits, inclination gauges, and digital CD-recording cameras, later replaced with high-density memory-card cameras, were used. Rapid access and portability were the basic requirements, in addition to all data being digital for rapid turn-around of information output.

It has been the general belief in the American Southwest that petroglyphs and pictographs (painted versions of the carved petroglyphs) were the creation of the Anasasi, who inhabited the region some 800 years earlier. Only after methodologies matured for dating leached pigments in pictograph rock that scientists discovered that these objects stretched back some 7000 years in time [17]–[21].

Once data was being acquired, it became clear that, upon plotting the coordinate locations, a consistent element of directionality was present. This is impossible to discern in the field because of a constant sweep of light across the sky from Earth's rotation and the general loss of exact direction while climbing arduous and dangerous terrain. Many times, we thought our transits, compasses, and GPS receivers faulty. Not once in the field did we think that we had not found data that invalidated previous directionality trends.

But the primary reason that directionality cannot be discerned in the field has to do with the nature of radiation flow.

Radiation flows like water in a channel, and Earth-to-space channels on a global scale cannot be seen at eye-level. Kilometers of elevation are needed, particularly when the terrain elevation increases kilometers to the south. The first indication that a preferred channel toward polar south is evident in petroglyph-site locations came from aerial and satellite photography.

In this paper, we shall make reference to angles of inclination and "blinders." The angle of inclination is that angle off-horizontal (0°), where the observer can first see the skyline. If looking downhill, the inclination angle will be negative, while looking uphill gives a positive angle of inclination (cf. Section XIII).

A "blinder" is an object in front of the observer that blocks a portion of the sky in the FOV. A blinder can be higher terrain, either close by as looking uphill, a mountain or mountain range either close by or tens of kilometers away, a boulder in front of the viewer, or the east or west sides of a canyon or escarpment wall.

In the northern hemisphere at mid-latitudes, blinders block the intense synchrotron light from the center of plasma columns located near polar south. This is always outside a blocking cone of about $\pm 4^\circ - 8^\circ$ of polar south (measured with allowance for the local magnetic declination on the compass). A petroglyph on, for example, an east-facing panel will usually have a north–south offset of $176^\circ - 356^\circ$, while on a west-facing panel, the north–south offset is $4^\circ - 184^\circ$.

At mid-latitude in the northern hemisphere, the angle of inclination for polar south at petroglyph locations will range from about $+24^\circ$ to $+31^\circ$. The angle of inclination and the plane of the blinder are latitude dependent.

The southern hemisphere has the same inclination-blinder dependence as the northern hemisphere to about 25° S. At more southerly latitudes, the angle of inclination changes, as does the plane of the blinder, showing an eastward bend of the plasma column away from Antarctica.

Once the preferred directionality and inclination-angle-horizon dependence was known, approximately 500 petroglyphs could be found and logged in a week. But equally important in finding where the petroglyphs are is where they are not. Some 75% of our time in the field was spent searching "where they are not."

The logging expanded worldwide with team members traveling to all continents (except Antarctica) and the GPS loggings of numerous contributors from around the globe.

Our most useful guide books turned out to be some of the oldest: Mallery, 1888 [22] and the 1960 work of Loring and Loring, 1982 [23].

B. Data Plotting

The plotting of some 500 weekly petroglyph coordinates and the recording of images involved many computers, ranging from the Los Alamos National Laboratory "Q" machine [2001; 30 teraOPS (trillion operations per second) and two trillion bytes of memory] to simple laptops suitable for use in the field.

Some dozen different software programs, both laboratory and commercial, were used to put recorded locations on topographical maps, aerial, and satellite photos, preferably with 3-D mapping capabilities.

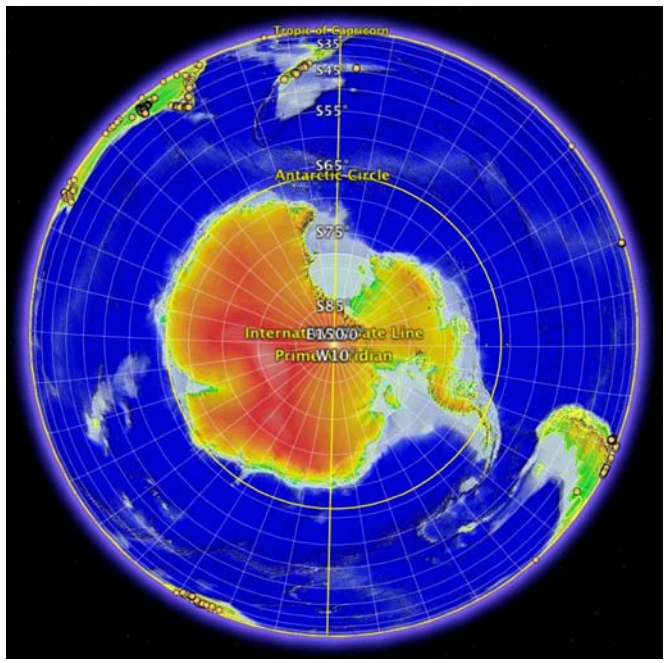

Fig. 1. Antarctica map distribution of petroglyphs. Upper left: South Australia and Tasmania. Upper center: New Zealand. Upper right: Easter Island. Lower right: Chile and Argentina. Lower left: South Africa. The yellow and red dots are GPS-logged petroglyph and pictograph sites, respectively. Brown denotes high altitudes while green denotes low altitudes.

The Los Alamos National Laboratory, Information, Records, and Media Services provided a helicopter for 400-ft (122 m) altitude photo/video recordings of petroglyph areas on the 46-mi^2 $(121\ \text{km}^2)$ laboratory facility, invaluable for future site-equipment calibration.

III. Global Distribution of Logged Petroglyphs

A. Antarctic Regions

Antarctica (Fig. 1) is among the most important regions of study, as it will be shown that the intense REBs from major solar outbursts enter Earth's ionosphere from space preferentially above this $14 \times 10^6\text{-km}^2$ land mass.

As a continent, it is also the most isolated: An "island" immediately surrounded by a single ocean and also by the other continents that lie beyond the horizon. In comparison, the Arctic (Fig. 2) is rich in observational terrain.

The closest areas logged to study the Antarctic phenomena included Pitcairn Island (25.2° S, 130.0° W), Easter Island (27.1° S, 109.5° W), South Africa (30.8° S, 23.1° E), Monte Aranda, Chile (32.11° S, 71.08° W), Scott River, Australia (33.7° S, 116.2° E), Flinders Ranges, South Australia (35.0° S, 138.5° E), Victoria, Australia (37.6° S, 148.7° E), Tasmania (43.9° S, 146.6° E), Chatlan Islands (44.0° S, 175.6° E), and South Island, New Zealand (45.99° S, 168.24° E).

B. Arctic Regions

In contrast, the most remotely known logged sites in the northern hemisphere include Mull Island (Trømso), Norway (56.36° N, 6.19° W), Cape Alitak, Alaska (57.0° N, 154.5° W),

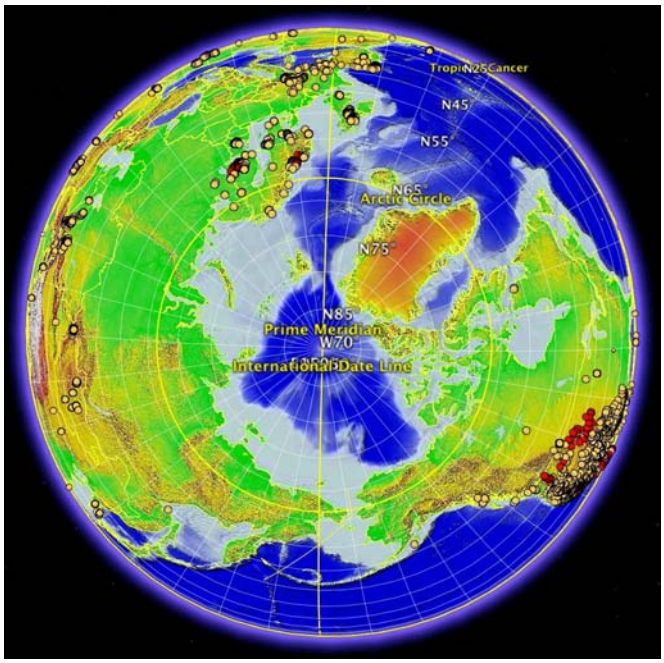

Fig. 2. Arctic map distribution of petroglyphs and pictographs.

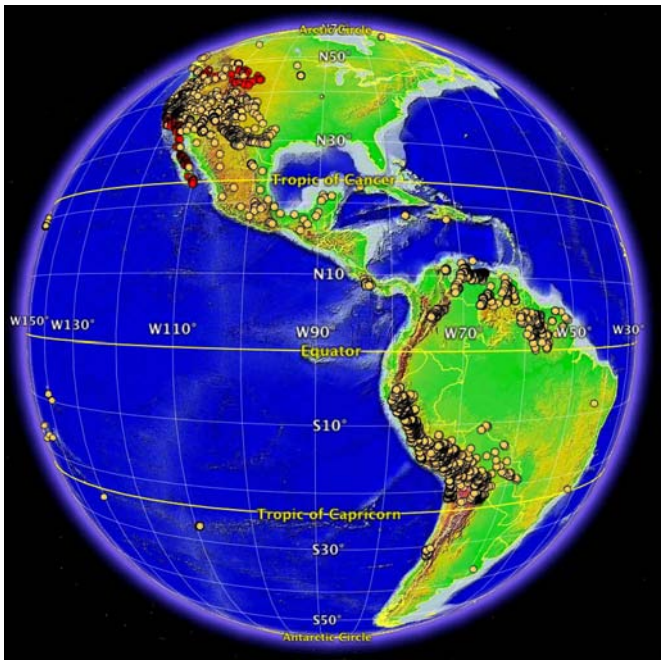

Fig. 3. Petroglyph and pictograph distributions for the North and South America continents. Longitude 30° W–150° W.

Kangiqsujuaq, Quebec (61.4° N, 58.3° W), and Soroya, Norway (70.7° N, 22.5° E) (Fig. 2).

C. Earth's Azimuthal Distributions, Global Latitudes $\pm 50°$

Figs. 3–6 show the distribution of known petroglyph sites on the North and South American continents longitude 30° W–150° W; Europe, the Middle East, and Asia; the African Continent and adjoining regions, longitude 90° E–30° W; and part of Southeast Asia, Indonesia, Micronesia, Melanesia,

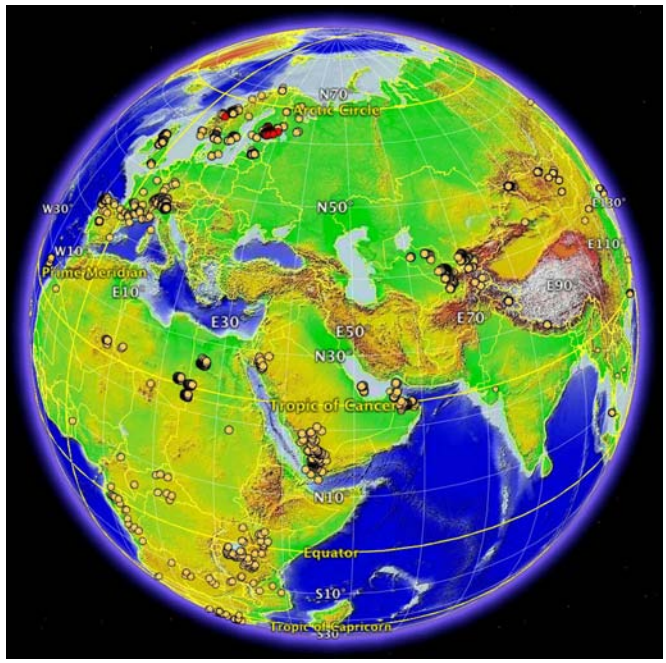

Fig. 4. Petroglyph and pictograph distributions for Europe, Middle East, and Asia. Globe centered on the Tropic of Cancer.

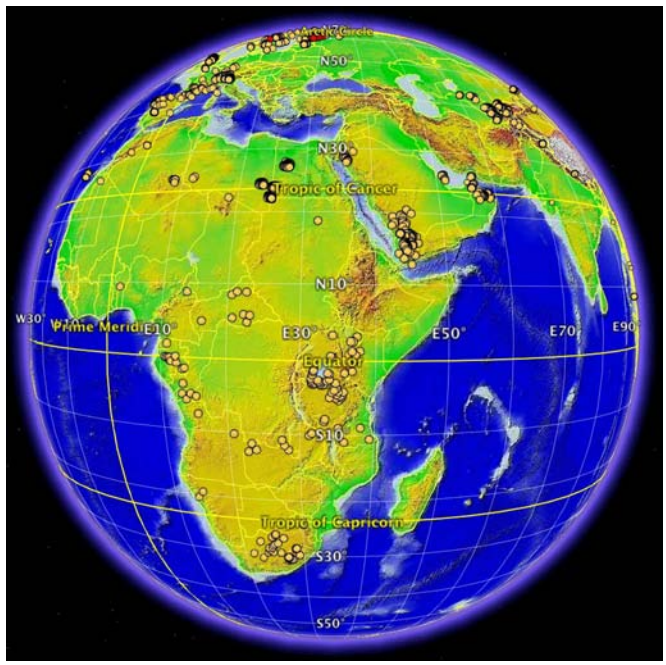

Fig. 5. Petroglyph and pictograph distributions for the African Continent and adjoining regions. Longitude 90° E–30° W.

Australia, New Zealand, and Polynesia, respectively, longitude 150° W–90° E.

IV. Pacific Islands

The South Pacific encompasses 40 million km^2: from Hawaii in the north, Easter Island in the East, New Zealand in the south, and Belau in the west; an area three times the size of Europe. This region includes Micronesia, Melanesia, and Polynesia (30° N– 45° S, 140° E–110° W) with some

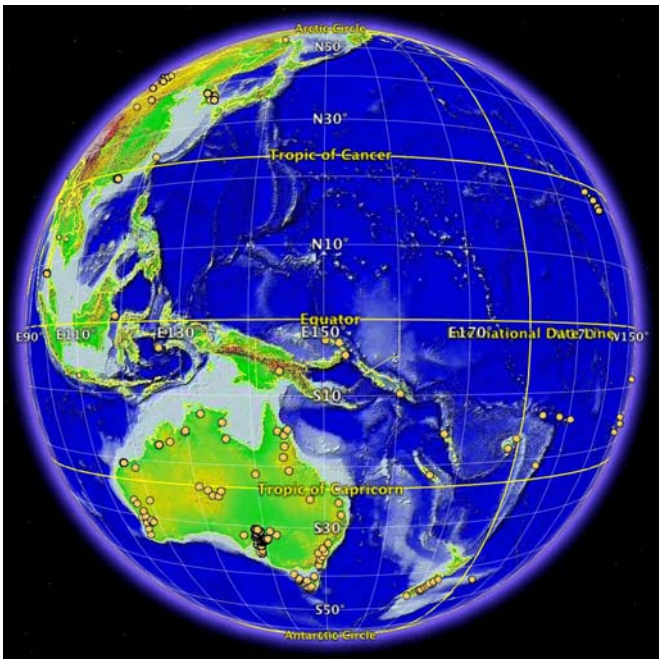

Fig. 6. Petroglyph and pictograph distributions for part of Southeast Asia, Indonesia, Micronesia, Melanesia, Australia, New Zealand, and Polynesia. The Hawaiian Islands are located on the horizon, upper right. Longitude 150° W–90° E.

7000 islands total. The number of known petroglyphs sites number tens of thousands with more than 7000 petroglyphs listed in the Marquesas Islands group (French Polynesia) alone.

Among those places where petroglyphs are recorded include Borneo; Chatham Islands; Easter Island; Fiji; Fitiuta, Ta'u Island (American Samoa); Gilbert Islands; Guadalcanal (Solomon Islands); Hatiheu Valley, Nuku Hiva (Marquesas); Hawaiian Islands (Sandwich Islands); Kai Kecil (Moluccas); Lapita; Leone, Tutila Island; New Caledonia; New Guinea; New Hanover; Pitcairn Island; Pulao Ogar, Pulau Arguni, MacCluer Gulf (Papua, New Guinea); Society Islands; Tabar (New Ireland); Tahiti; Telekitonga (Tonga); and Vanuatu.

Almost all of the markings in this region are rock engravings, i.e., petroglyphs; pictographs are rare.

Following the classifications of our logging data, we shall group petroglyphs from New Zealand, in Polynesia, with those of Australia and Tasmania.

A. Pitcairn Island

Pitcairn Island (25.1° S, 130.2° W; 4.5 km^2) lies on the Tropic of Capricorn, 7200 km from Earth's southern axis. The one site that has been surveyed, "Downrope," is in a cove on vertical rock above a sandy beach; Pitcairn's only beach. At this location, the petroglyphs have a distinct south FOV (SFOV), as shown in Fig. 7 (cf. Section XIII).

For film-photography illustration, the petroglyphs have been "chalked in" for visibility; a practice no longer used today. It is meaningful that one of each major petroglyph type is found at Downrope.

1) Easter Island: Easter Island (27.5° S, 109.5° W; 166 km^2) lies 7000 km from Earth's southern axis. Some

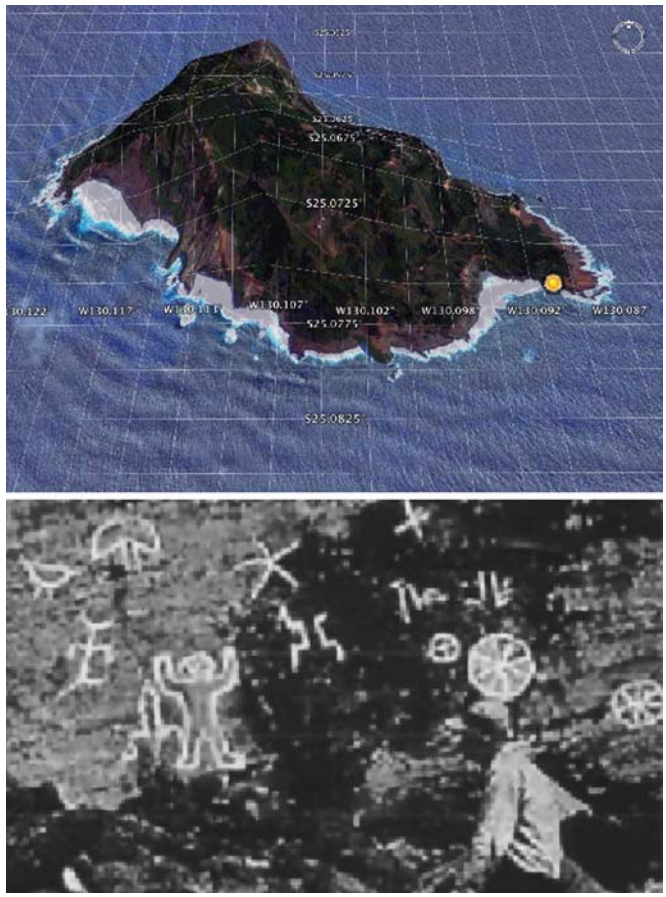

Fig. 7. Pitcairn Island (25.1° S, 130.2° W). Top: Oblique topographic with the site marker at the far eastern tip of the island named "Downrope." Bottom: Petroglyphs at Downrope.

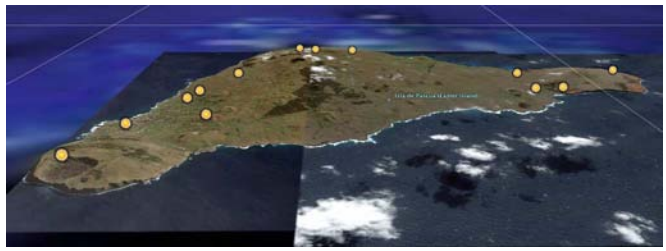

Fig. 8. Easter Island (27.1° S, 109.4° W; 24-km length). Far left: Rano Kau crater. Puakatike (Puoa Katiki) crater, second site from right. The three sites in the middle are centered on north–south channels through hills. With other sites on the northern wall of craters, all known petroglyphs are SFOV.

4300 petroglyphs have been documented on Easter Island, clustered at the sites marked in Fig. 8.

B. Hawaiian Islands

Typically, the Hawaiian Islands, a chain stretching 2400 km, are delineated in two parts, small islands that make up the northwestern (Leeward) group and the larger or southeastern (Windward) islands. Petroglyphs are found in large numbers on the southeastern islands of Hawai'i, Maui, Kaho'olawe, Lana'i, Moloka'i, O'ahu, Kaua'i, and Ni'ihau. The distribution of petroglyph sites on the southeastern islands is shown in Figs. 9 and 10. Those on Moloka'i, O'ahu, and Maui have not been plotted.

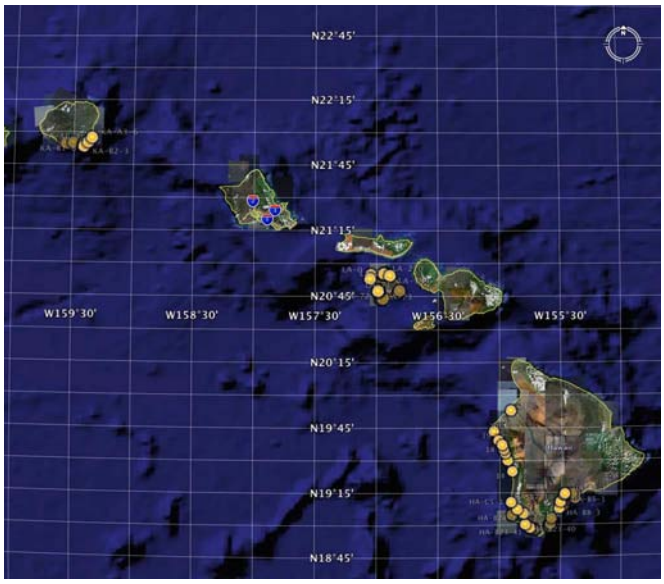

Fig. 9. Hawaiian Islands (18° N–22° N, 155° W–160° W; 600-km length). Not plotted are logged sites on Molokai, Oahu, and Maui.

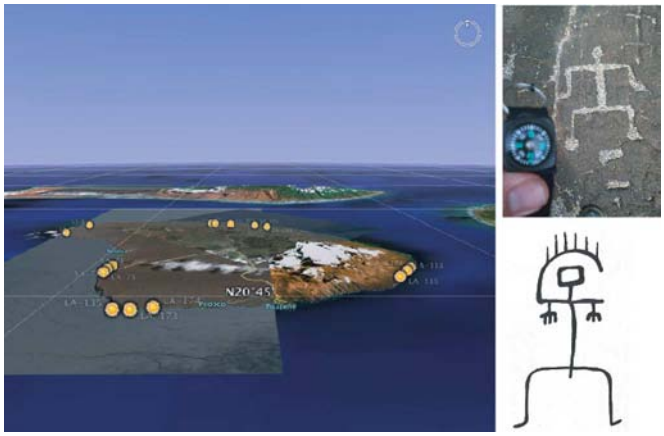

Fig. 10. Lanai, Hawaii. Two selected Puako petroglyphs, Pele at the bottom, are shown on the right.

V. Asia and Southeast Asia

A. Thailand

Because of terrain and foliage, petroglyphs sites in Thailand were difficult to survey. Our survey sites included Tham Nak (Naga Cave), Ao Phang-Nga Marine National Park, Tha Dan (pier), James Bond Island, Ko Panyi, Tham Lod, and Khao Khian (Fig. 11).

B. South Korea

The South Korean sites logged were Sugok-ri, Imdong-Myeon, Andong-si, Gyeongsangbuk-do, Bangudae, Daegok-ri, Eonyang-eup, Ulju-gun, Ulsan, Bangud, Cheonjeon-ri, Cheonjeon-ri, Dudong-myeon, Ulju-gun, Ulsan, Yangjeon-dong, Janggi-ri, Goryeong-eup, and Goryeong-gun. While Fig. 12 shows only the particular site location, several of the sites consisted of long north–south-oriented rock areas with numerous petroglyphs.

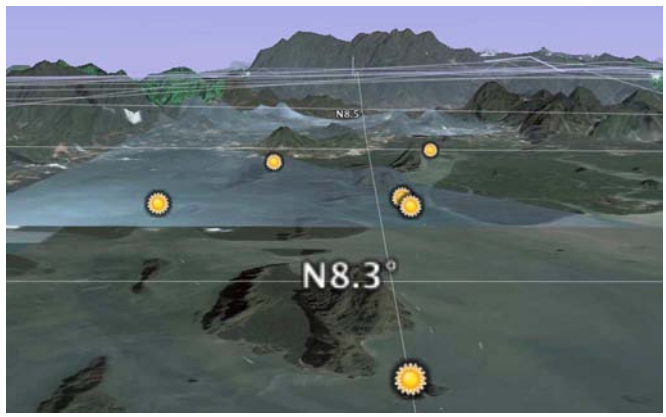

Fig. 11. Thailand (8.3° N, 98.5° E). From front to back, Thamna, James Bond, Kopany and Khaokh, Thamlo, and Thadan islands.

C. Hong Kong, Hong Kong

The logged coordinates of Shek Pik, Cheung Chau, Wong Chuk Hang, Big Wave Bay, Po Toi, Tung Lung, Lung Ha Wan, and Kau Sai Chau are shown in Fig. 13.

D. China

Chinese petroglyphs are little known internationally [24]. Our database of logged Chinese sites is minimal even with our own surveys in Thailand, South Korea, and the regions of Central Asia surrounding China. However, petroglyph sites in China are numerous with most concentrated along the Yellow River and Yangtze River Valleys with adjacent north–south running mountain ranges suitable for carving petroglyphs. Known petroglyphs are concentrated along these ranges: the Yinshan (Yin Mountains) of Inner Mongolia and the Helanshan (Helan Mountains) of Ningxia (Fig. 14).

Documented sites in three general areas include: the Yinshan at Urad Rear Banner (Dishui Gou and Bu'erhan Shan), the Yinshan at Dengkou county (Ge'er'aobao Gou and Molehetu Gou), and the Helanshan area (Heishimao, Shizuishan City; Daxifeng Gou, Pingluo County; Helankou, Helan County; Siyanjin, Qingtongxia City; and Gujingou).

Six sites have been documented along 75 km of the Zhuozi Mountains, running north to south. The petroglyphs of Zhaoshaogou are located on the southern slopes, 15-km southeast of Wuhai. The petroglyphs at Kucaigou are primarily along the southern escarpment. Some are located on northern cliffs, but their inclinations have not been measured, as is also the case for the Subaiyingou petroglyphs. Petroglyphs at Mao'ergou are located along the southern escarpment.

There are 19 more sites documented in the Helan Mountains including Mairujing, Fanshigou, Greater and Lesser Shoulingou, Hongguozikou, Heishimao, Jiucaigou, Guotougou, Baijigou, Great and Lesser Xifenggou, Baitougoum, Helankou, Suyukou, Huohuogou, Kujinggou, and Damaidi.

Petroglyphs in the central and northern parts of the Helan Mountains predominantly face south or east. Petroglyphs on the escarpments of the Weiningbei Hills, south of the Helan, all face south.

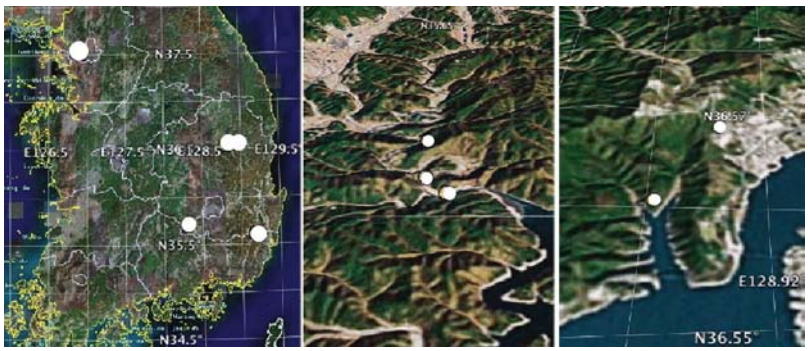

Fig. 12. South Korea. From left to right: Frame 1: Mainland. Frame 2: Daegok-ri, Eonyang-eup, Ulju-gun, and Ulsan. Frame 3: Sugok-ri and Imdong-Myeon.

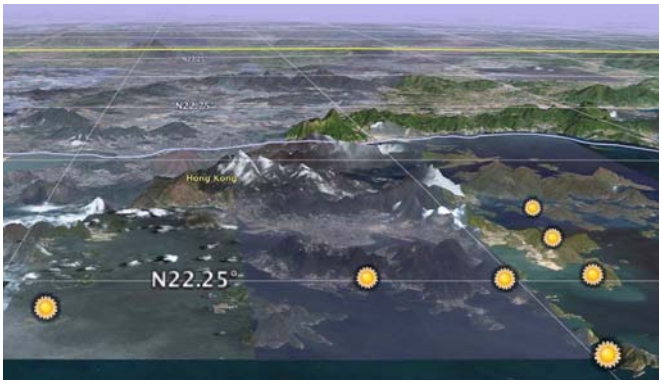

Fig. 13. Hong Kong, Hong Kong (22.28° N, 114.15° E).

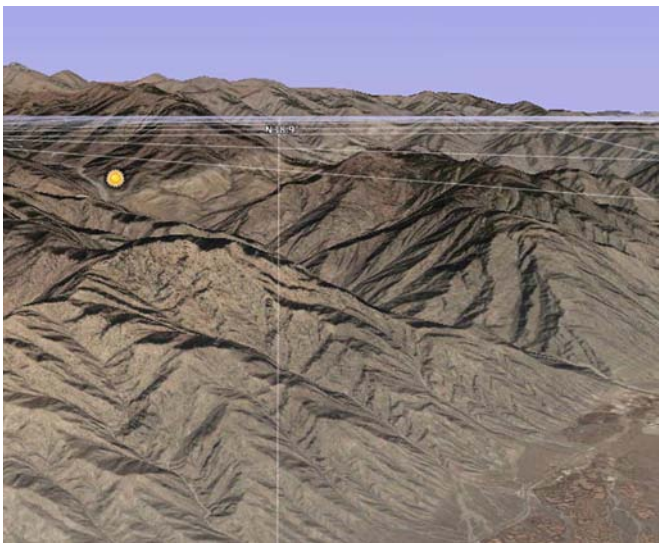

Fig. 14. Helanshan Mountains, China (38.7° N, 106.0° E). While this mountain range has some 36 known sites, we have coordinate data for only one.

The available petroglyphs in Huashan are located in Ningming County (Zuojiang). Some 1800 petroglyphs have been photographed on the cliffs along the Guangxi River.

The GPS locations of a few of these sites are known but are absent of FOV and inclination. With this exception and allowing for the lack of inclination data for some sites, all logged Chinese petroglyphs are SFOV.

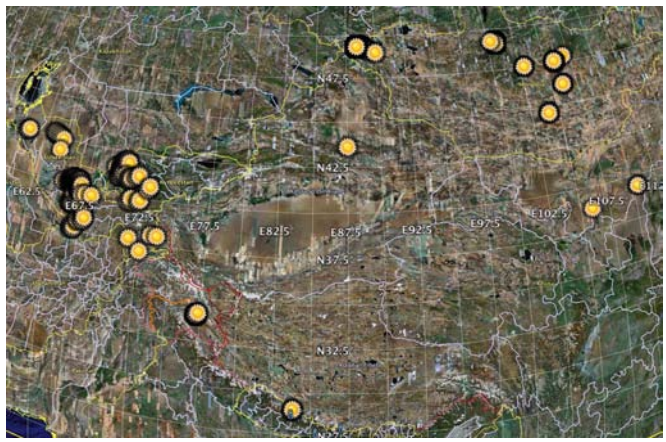

Fig. 15. Mountain Regions of Central Asia, 30° S–50° S, 60° E–110° E. From left to right: Uzbekistan, Tajikistan, Kashmir, Nepal, and Mongolia. The two topmost site areas, from center to right are Altai, Mongolia, and the Chuluut River region, Mongolia. Altai is the corner of four countries, clockwise, Mongolia, China, Kazakhstan, and Russia.

E. Mountain Regions of Central Asia, 30° S–50° S, 60° E–110° E

Fig. 15 shows, from left to right, logged petroglyph sites in Uzbekistan, Tajikistan, Kashmir, Nepal, and Mongolia. All data plotted for Uzbekistan, Tajikistan, and Kashmir have SFOVs.

1) Altai, Mongolia: With information from the National University of Mongolia, we logged Altai, Mongolia in May 2006. Altai lies at the far northwest corner of Mongolia, where the borders of Kazakhstan, Russia, and China also meet.

The "operations center" was the town of Olgii, allowing ready access to the rough "steppe land" strewn with boulders, sun-dried bones, and free roaming herds of horses and yaks.

The usual array of spiral, concentric, "ladder," and "stick-men" petroglyphs [6] were noticeably absent as separate entities but instead incorporated into the cusps and antlers of deer, sheep, and other animals depicted in hunting scenes. This is not an uncommon occurrence and can be found at numerous sites throughout the American Southwest.

All petroglyphs had an SFOV (Fig. 16) and often traced the profiles of 3200-m mountains 17 km to the south. No petroglyphs were found when the altitude of these mountains reached 3600 m directly south of a recording site.

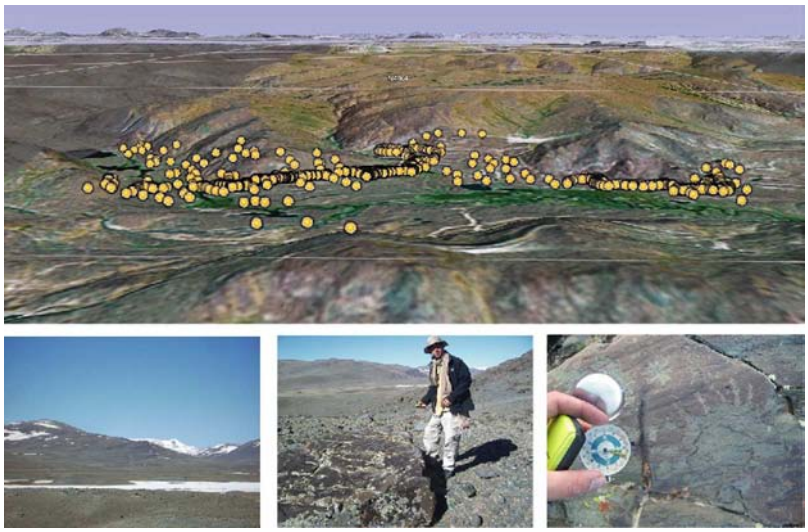

Fig. 16. Altai, Mongolia. Top: GPS survey of petroglyphs. The survey extends 7.25 km. Bottom left: Survey Area; Bottom center, One of the authors (AVS); Bottom right: Rayed petroglyph with compass reading. Altai lies where the borders of Kazakhstan, Russia, and China meet.

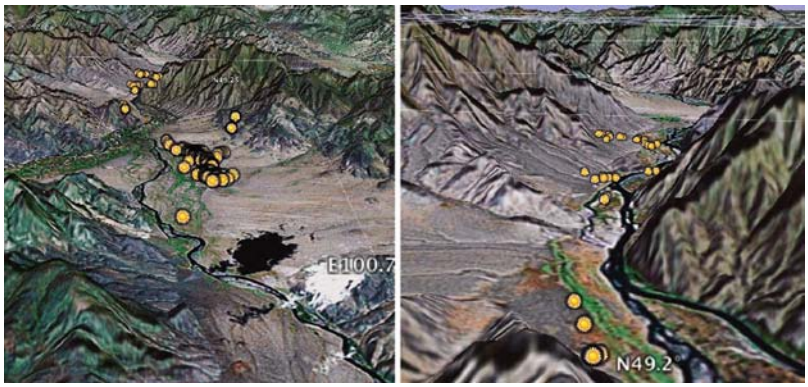

Fig. 17. Chuluut River Basin sites, Mongolia. Left: Southern end of the Chuluut River survey. Right: Northern end at the junction of the Chuluut/Ider and Selenge rivers.

2) Chuluut River Basin, Mongolia: Based upon earlier published logs and 3-D satellite and aerial data, we mapped out the most probable locations of petroglyph sites along the Chuluut River Basin in Central Mongolia, 1620-km northwest of Beijing.

To our great fortune, while logging the Altai site, we found that the Chuluut had already been GPS logged by a team from the University of Newcastle, the University of Edinburgh, and the National University of Mongolia from July 11 to September 15, 2004. The purpose of this expedition was to locate and record petroglyph sites in the Huremt district, Arkhangai province, through which the Chuluut flows.

The survey area started where the Chuluut/Ider river meets the Selenge River (49.26° N, 100.67° E; 1175 m) and ended near a lake at 49.10° N, 100.71° E; 1210 m, with a linear distance of 17.8 km.

The entire river plain lies within a channel defined by a north–south-oriented 1800-m mountain range to the east and a series of 1900–1400-m west–east ridges tapering to the east and ending at the Chuluut.

The northern sites (49.26° N–49.20° N) are primarily on the west side of the river and located on a mild east-facing slope near the Selenge.

The southern sites (49.16° N–49.13° N) run along an escarpment on the east side of the river.

All Chuluut River petroglyphs have an SFOV (Fig. 17). Individual boulder locations and a 1300-m mountain to the south determine the northern site inclinations. The inclinations for the southern sites are determined by a 1500-m mountain range to the south, 49.05° N.

These findings validated our initial site-location analyses, although we found out that our predictions were often tens of meters off the *in situ* GPS readings.

3) Nepal: Because of its abundance of suitable rock material, 3000-m valleys, and high mountain elevations of 6000 m, Nepal offers well-defined FOVs, as shown in Fig. 18.

4) Uzbekistan, Tajikistan, and Kashmir: Uzbekistan, Tajikistan, and Kashmir also offer an abundance of petroglyph-rock palettes and a large number of petroglyphs (Fig. 19).

VI. India

While Pakistan and Afghanistan, rich in petroglyphs, have been heavily surveyed, our own data have not yet covered these countries. Instead, we have concentrated on the Great Himalayan Range in neighboring India.

Fig. 18. Nepal. Left: Sites at Samar, Tatang, and Kak Nyingba. The sites are located in a north–south "channel" on the Kaligandaki River, the deepest river gorge on Earth. Each is situated with an SFOV through gaps in the mountain range (bottom of picture). Right: View of the Kaligandaki gorge, 325-km northwest of Mt. Everest.

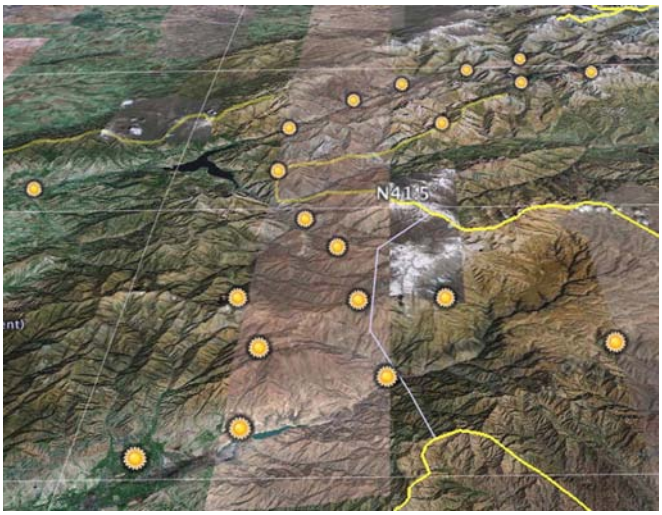

Fig. 19. Uzbekistan, 41.5° N, 70.5° E. Each site is situated in a gorge or location with an SFOV.

A. Zanskar River, India

To date, our loggings have been taken on the Zanskar River, running between the Zanskar and Great Himalayan Ranges (Fig. 20). The headwaters of the Zanskar are at 4300 m, flowing through steep gorges until its confluence with the Indus River at 3100 m. Precise FOV and orientation have been taken in the very limited gorges or "channels" in the Himalayan Mountains. All have an SFOV.

Note the very narrow beam of sunlight from a southerly direction illuminating the steep mountain slopes (Fig. 21).

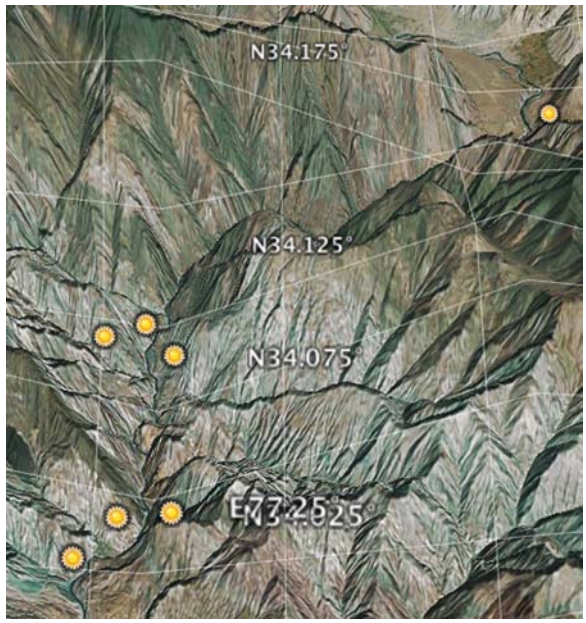

Fig. 20. Petroglyph sites along the Zanskar River close to where it flows into the Indus River. As shown, each site have an SFOV.

Fig. 21. Photograph of the Zanskar River looking down to one of the petroglyph sites illuminated by a narrowband of sunlight.

VII. Middle East

The Middle East and surrounding regions are locations rich in petroglyphs. In spite of our large collection of photographs from Pakistan and Afghanistan and less so for Turkmenistan, Iran, Iraq, Syria, Turkey, sites in Saudi Arabia, Yemen, Qatar, United Arab Emirates (UAE), and Oman have been well cataloged and plotted (logged data from Har Karkom, Negev, Israel, have not yet been plotted on our maps).

In Saudi Arabia, the sites located at Tabuk in the north and the Yemen sites are located primarily in the volcanic Asír–Yemen highlands. These also border and lie within the Rub' Al Khali and Nafuo Dahi regions. Two more sites in Yemen are along the Kaur Mountains coastal range (Fig. 22). All sites have an SFOV.

The sites in the UAE and the Musandam Peninsula are located to the far north in a geographically complex mountain range at the Strait of Hormuz, providing excellent FOV information.

The petroglyph sites of Oman are principally in a narrow mountain range defining the UAE and Oman border in the north and also in the well-defined Jebel, Akhdar Mountains (Fig. 4).

Fig. 22. Saudi Arabia and Yemen petroglyphs sites (28.15° N, 36.40° E).

Fig. 23. Boukerkour, Morocco, petroglyph-site location (31.1° N, 4.8° W).

VIII. Africa

A. North Africa

Sites in the Western Sahara, Morocco (Figs. 23 and 24), Algeria, Libya, and Sudan are shown in Figs. 4 and 5. The site in Sudan is located at the Fourth Cataract Dam construction site near Meroë (single marker, 8-o'clock position, Fig. 4). It is on an eastern panel along a north–south stretch of the river with an SFOV (18.69° N, 32.06° E).

Other surveyed regions in the Libyan desert include sites around Akakus and the Gilf Kebir region. The Gilf Kebir includes the central Libyan Desert, Jebel Almásy, The Northern Gilf Wadis, Wadi Abd el Melik, The Southeastern Gilf Kebir, Wadi Bakht, The Southern Gilf Kebir, Jebel Uweinat, Karkur Talh, and Jebel Arkenu.

The Jebel Arkenu (22.256178° N, 24.702987° E) contains numerous petroglyph sites, as shown in a portion of this concentric crater (Fig. 25). While we obtained current GPS-surveyed loggings of the Libyan Desert, other data came from 1930-era terrain surveys. The "rectangular" appearance of some locations are an artifact of 80 km × 60 km survey areas from 1970–1980-era Soviet military aerial maps of the Eastern Sahara.

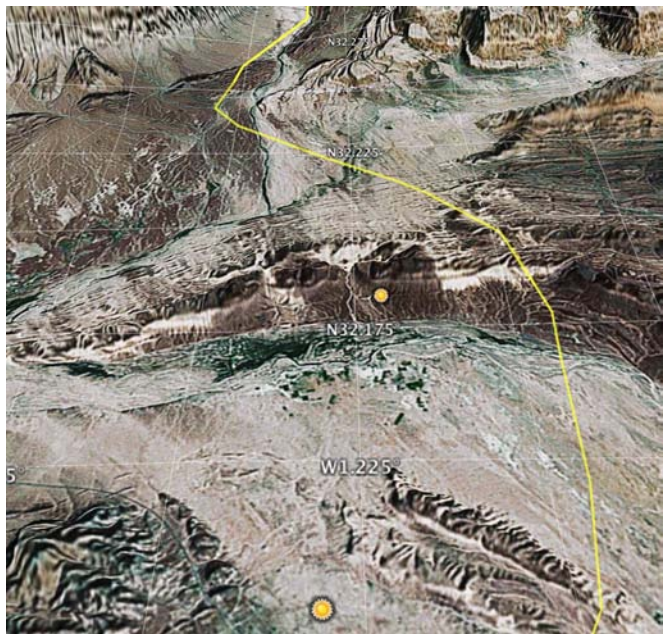

Fig. 24. Figuig Mountain, Morocco, petroglyph-site locations (32.1° N, 1.2° W).

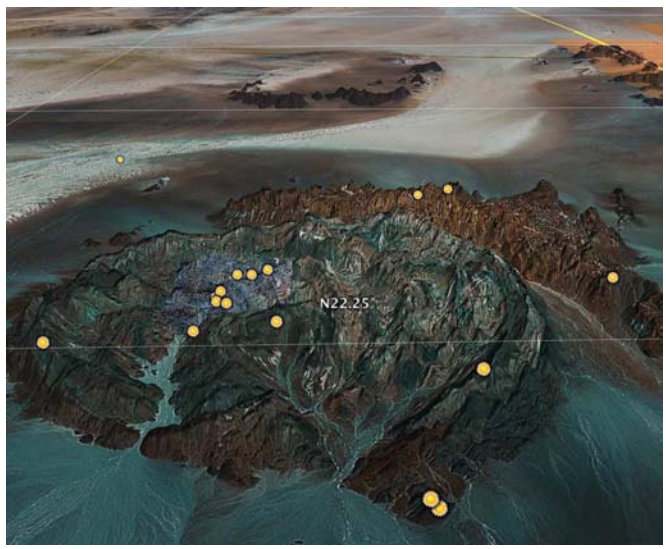

Fig. 25. Jebel, Arkenu, Libya, sites (22.25° N, 24.70° E).

B. Central Africa

Logged sites in Benin, Cameroon, Central African Republic, Equatorial Guinea, Gabon, Congo, and the Democratic Republic of the Congo are shown in Fig. 5.

C. Southern Africa

Logged sites in Angola, Zambia, Namibia, and South Africa are shown in Fig. 5. Limpopo, South Africa, is a site of ongoing survey.

Fig. 26. Canary Islands of El Hierro (front) and La Palma (rear) with marked petroglyph sites, 28.7° N, 17.7° W. The "gray" area in front of La Palma is part of a map overlay on the ocean.

Fig. 27. Aerial view of the Southern Alps.

D. Canary Islands

Logged petroglyphs sites on the islands of La Palma and El Hierro are shown in Fig. 26 (the gray area in front of La Palma is the ocean, the color change resulting from a high-detail aerial photo overlaying the satellite image). All sites have an SFOV.

IX. Europe, Scandinavia, and the United Kingdom

Our logged data from Europe included sites in France, Spain, Switzerland, Liechtenstein, and Italy. Most of our surveys were in the southern Alpine mountains (Fig. 27), particularly in the Camonica Valley, Italy.

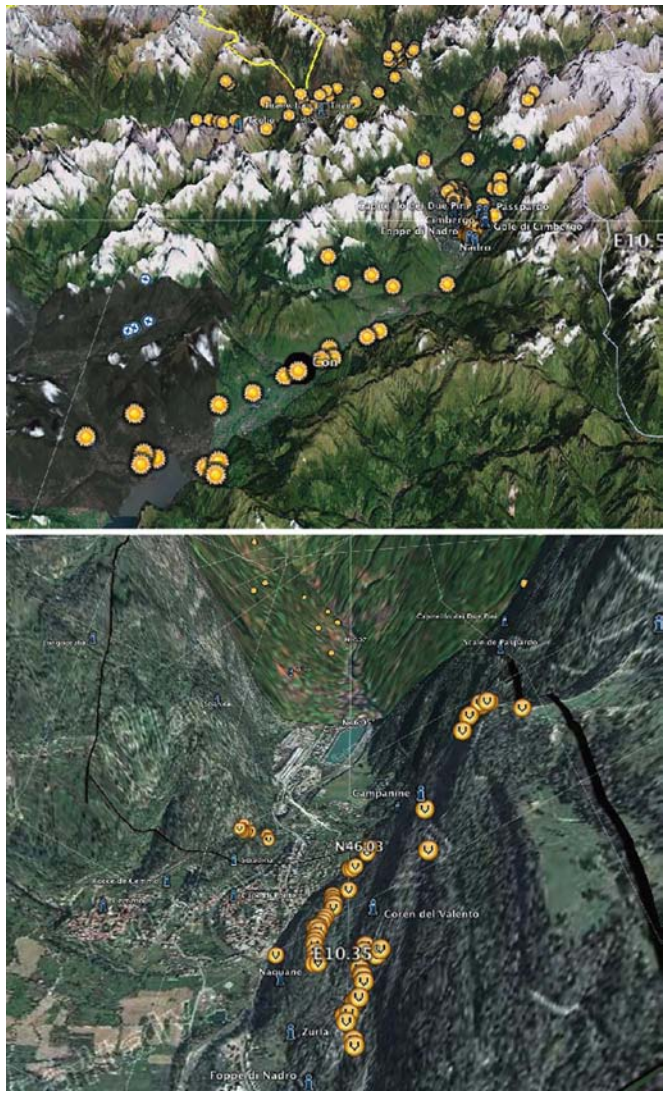

Fig. 28. Top: Valcamonica and Valtellina alpine distribution of sites. Note that the white areas are not clouds but rather snow-capped peaks with petroglyphs located to the south side. Bottom: Capo di Ponte, Sellero, Ceto, Cimbergo, Paspardo, and Naquane sites. The black north–south lines are artifacts from piecing aerial photographs onto a satellite photo background.

A. Valcamonica

The top of Fig. 28 shows the distribution of petroglyphs in Valcamonica and Valtellina. Our surveys in Valcamonica were in the vicinity of Capo di Ponte (46.03° N, 10.34° E) (Fig. 28, bottom). These included sites at or near the towns of Tirano, Teglio, Sellero, Capitello dei Due Pini, Perseghine-Pozzi, Longoprato, Zurla, Coren del Valento, Campanine, Naquane, Scianica Seradina, Rocce de Cemmo, Gole di Cimbergo, Le Santa-Pié, Scale de Paspardo, Passpardo, Cemmo, Nadro, Cimbergo, and Foppe di Nadro.

Coordinates for individual petroglyph boulders and sites farther south are shown for the Darfo–Luine region (Fig. 29).

B. Spain

In Spain, our donated data primarily focused around the Extremadura (Molino Manzanez) and Levantine regions to the

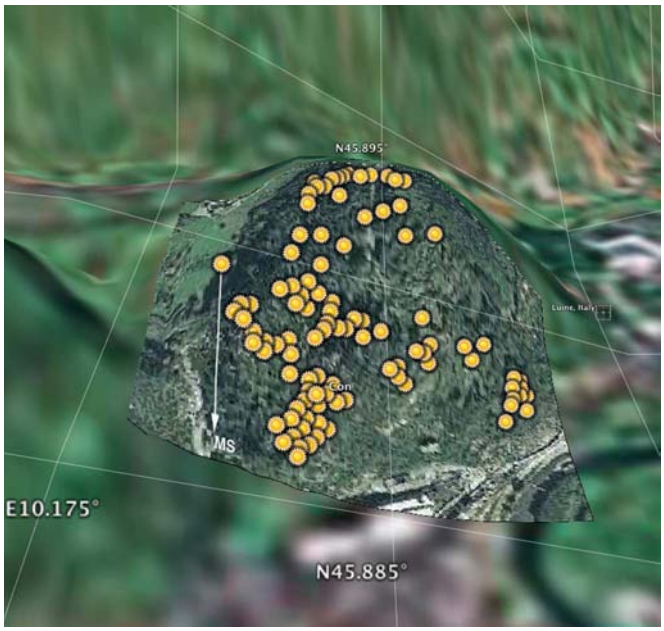

Fig. 29. Luine–Darfo site. Valcamonica, Italy. The northeast–southwest running eastern slope of the Camonica Valley (right) provides a 27° blinder directly south of this site, although the geology of the location provides *in situ* blinders.

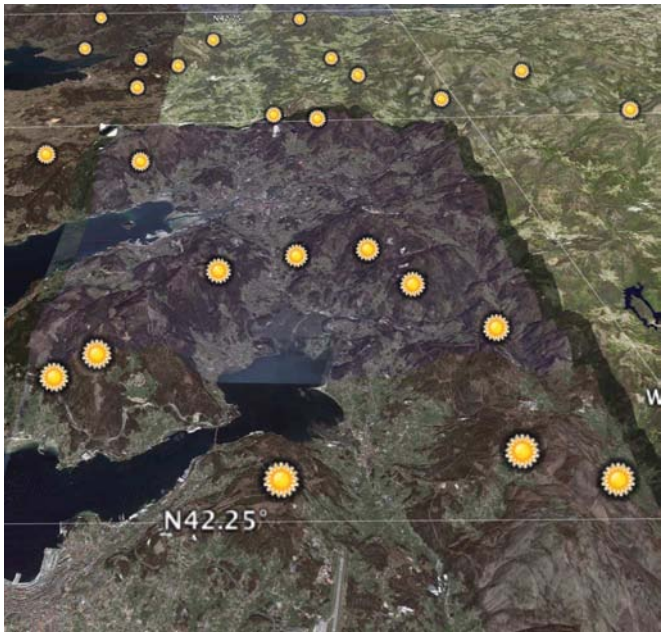

Fig. 30. Galicia region, Spain, 42.9° N, 8.7° W.

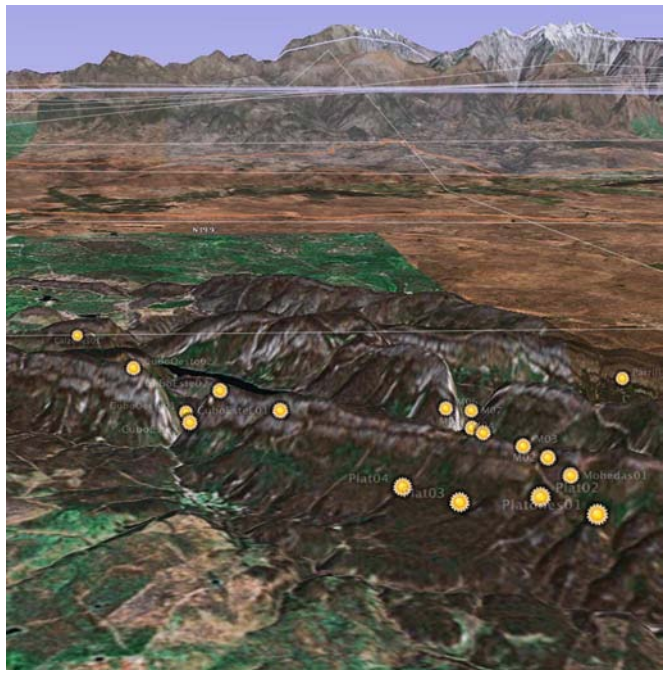

Fig. 31. Parque Monfraque, Spain, 39.7° N, 5.5° W.

Fig. 32. Finland. Portion of the pictograph and petroglyph region centered on 61° N, 27° E.

south and southeast, as well as Galicia to the north. Our surveys also included Parque Monfrague.

An abundance of Galicia petroglyph sites exist in the usually northeast–southwest-oriented rows of mountain ridges, as shown in Fig. 30 between the Rio Lerez, Rio Tea, and Rio Miño in the vicinity of Muros, Porto do Son, Rianxo, Bamio, Moraña, Campo Lameiro, Pontecaldelas, Tetón, and Arbo.

Data from Parque Monfrague was exceptionally good for orientation readings because of its multiple placements of hills and valleys along the Rio Tajo (Fig. 31).

C. Scandinavia

Our data for Scandinavia include Norway, Sweden, and Finland. Fig. 32 shows a portion of logged Finland sites, all located on the south sides of the mountain ranges. Finland has an appreciable number density of pictographs often barely visible.

The northernmost petroglyphs are at Soroya, Norway (70.57° N, 22.59° E), 700 km south of Svalbard Island (79° N) and 170 km northeast of Trømso (Figs. 2 and 4). On these maps, 73 km south–southeast of Soroya are the petroglyph sites on both sides of the rocky fjord at Alta (3-m elevation) has an

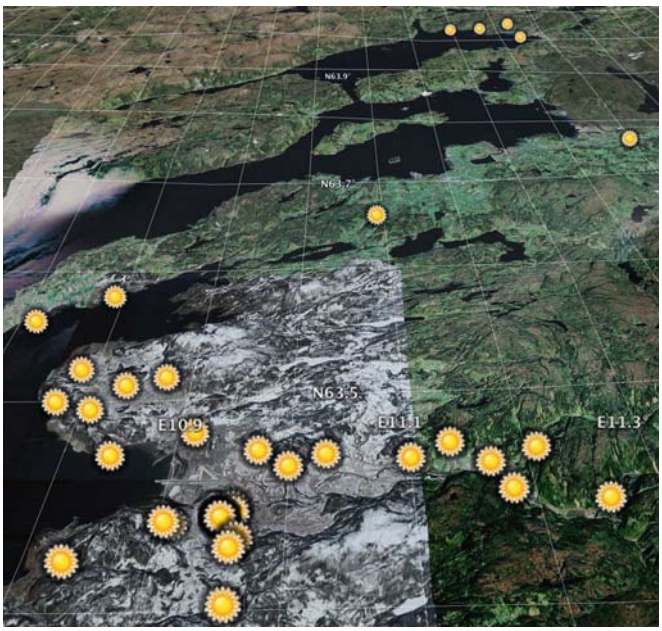

Fig. 33. Stjordalshalsen, Norway, 63.47° N, 11.03° E.

SFOV with a 400-m mountain blinder 5 km south and slightly west of this rich petroglyph area (not discernable on the globe).

The region in the vicinity of Stjordalshalsen, Norway, illustrates the SFOV characteristic of petroglyphs found in Scandanavia (Fig. 33). When the data is plotted on 1-m-resolution aerial photographs, the accuracy of this FOV is greatly enhanced.

D. United Kingdom

While an appreciable amount of data was donated from across the United Kingdom, most of the logged data shown in Figs. 2 and 4 came from Argyll, Lorn, Kintyre, Mull, Islay, Galloway, and the Isle of Man. The accuracy of data taken from these sites was excellent. The Argyll map Fig. 34 is typical of these sites.

All sites surveyed in Europe have an SFOV.

X. South America and the Caribbean

A. Caribbean

The Caribbean Islands have numerous petroglyphs. However, many are in mountainous areas and difficult to find because of foliage. As a result, most have been documented along the coasts (Fig. 3).

B. Northern South America

The northern South American Countries of Columbia, Venezuela, Guyana, Suriname, French Guiana, and northern Brazil have high densities of petroglyphs where the terrain has been logged.

On the eastern side of the coastal ranges and Andes, most have been logged along rivers, accessible by motor-powered log boats. The large boulder palettes along the banks are very limited in FOV, having none in north and very narrow channels

Fig. 34. Argyll, United Kingdom (GPS data courtesy of I. Tresman).

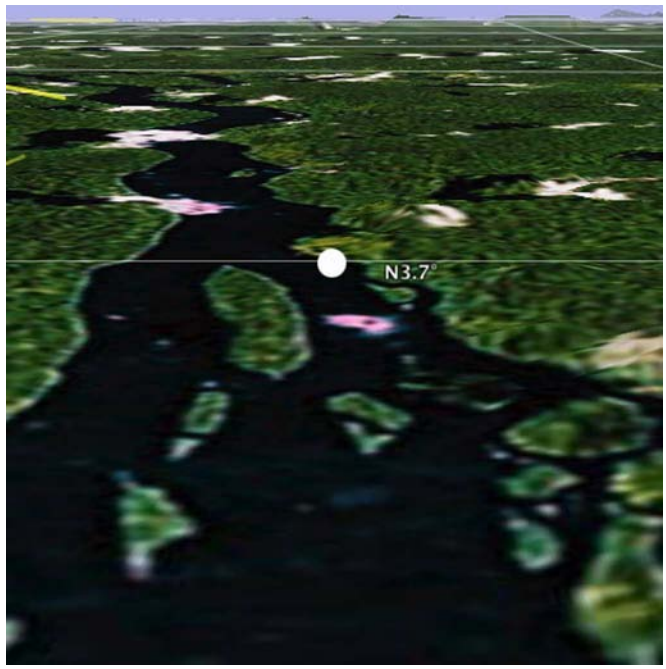

Fig. 35. Corantyn Sisa Creek, Suriname. While large boulders are found along the waterways, only those with an opening south have petroglyph carvings.

in south because of dense forest growth. This is particularly true in Suriname and Guyana, where Fig. 35 is typical of these sites.

C. Central and Southern South America

1) Peru and Bolivia: Petroglyphs sites from 4.6° S, 80° W to 23° S, 58° W (Peru, Bolivia, and northern Chile) are shown in Fig. 3. All are SFOV; most on southern slopes while others

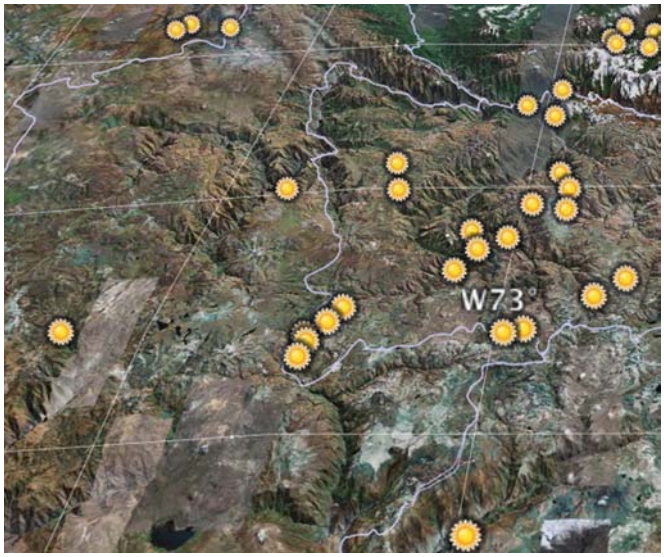

Fig. 36. Central Peru sites, 14.2° S, 73.2° W.

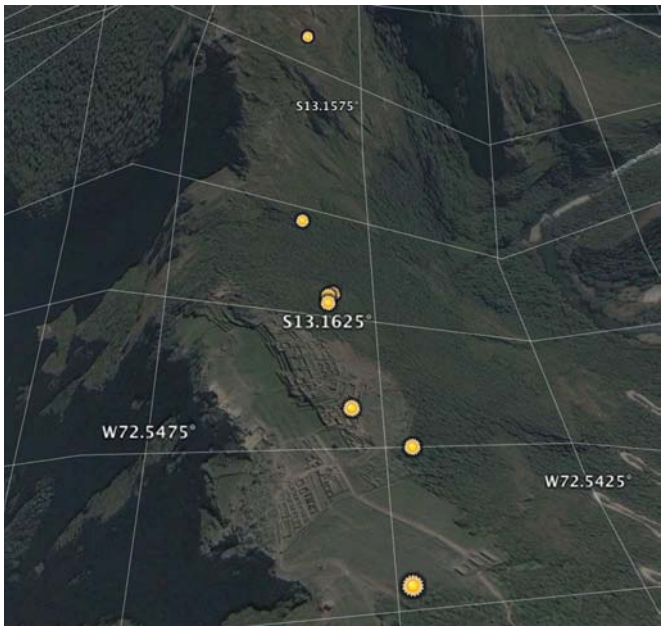

Fig. 37. Machuu Picchu, Peru sites. The petrogylphs are found on a north–south line between the 2634-m peak to the north (top), Waynapicchu, and a small 27° inclination mountain gap 180° (data: A. L. Peratt, and A. H. Qöyawayma).

look south from riverbank sites through very narrow mountain gaps. Central Peru, the area of our logging, is shown in Fig. 36.

Fig. 37 shows our Machuu Picchu sites. The petrogylph locations were predetermined by drawing a north–south line between the exact top of Waynapicchu, the 2634-m peak overlooking the ancient city from the north, and a narrow mountain gap, inclination of 27.3°, due south.

As shown, the petroglyph line cuts through the center of Machuu Picchu. All petroglyphs are carved on bedrock and not on the rock walls and structures.

2) Chile: Extensive and detailed surveys were made in Chile (Fig. 3) for petroglyphs, pictographs, and geoglyphs.

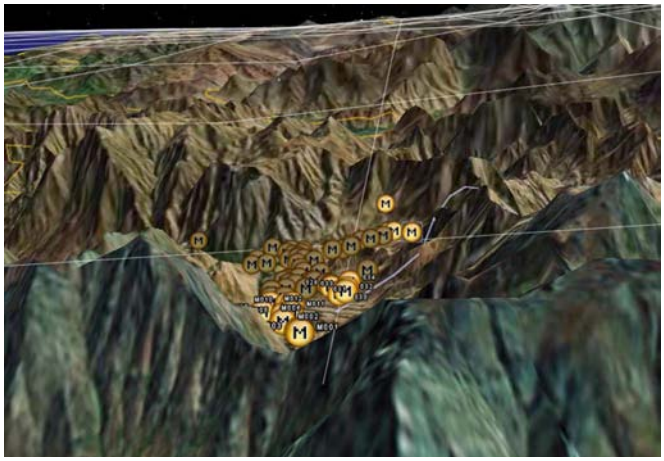

Fig. 38. Distribution of petroglyphs at El Mauro, Chile. The diameter of the El Mauro valley is approximately 10 km. (Data courtesy of P. Bustamante).

Chilean geoglyphs included the sites of Cerro Pentado, Chiza, Lluta Valley, Chacarilla, and the Tarapaca region.

The Tarapaca geoglyphs, located about 30 km from the coast (19° S, 70° W) are 10–20-km-long straight lines, running from mesa to mesa southwards. The lines are oriented in numerous directions.

Intermingled with the Tarapaca line geoglyphs are the Chiza geoglyphs, well-defined "giant petroglyphs" and kilometer-long straight paths running east, south, and west. The north–south line is 1.3 km long and runs along a western slope exactly polar south.

The geoglyphs are at the bottom of a canyon at the confluence of three canyons. The north, east, and west FOVs are blocked by steep slopes, while the geoglyphs SFOV are open with a slight hillside rise.

The Lluta Valley geoglyphs are on a 1.5-km-long north-facing hill, positioned approximately 250 m below the hillcrest with an SFOV.

It is the authors' opinion that these geoglyphs are the best crafted that we have seen.

The petroglyph/pictograph sites included Las Chilcas, San Pedro Viejo, Valle Ecantado, Arica, El Mauro, Monte Aranda, El Coligüe, La Ligua de Cogoti, La Toma, Cahuareche, Rio Acongua, Rosario, Huancarane, Pusharo, and other sites along the Illapel River; for example, Cuz Cuz El Sauce, Cuz Cuz Cerro Norte, Cuz Cuz Canal, Los Mellizos, Las Bellacas, Los Alamos Cespedes, and Bellavista.

Fig. 38 shows the site distribution at El Mauro. Like the other sites in Chile, these have an SFOV. Fig. 39 is an open-shutter photograph of petroglyphs silhouetted against the southern sky (31° S, 71° W).

XI. North America

A. Canada

British Columbia, Vancouver Island, and the Milk River, Alberta, were surveyed in Canada.

On Vancouver Island and the Milk River, 34 and 59 sites were logged, respectively. All had well-defined SFOV locations.

Fig. 39. Petroglyphs inscribed on the north face of boulders with an open-shutter recording of the southern sky. This form of recording on relatively mild north-slope boulders is found as far as 8° N (data courtesy of P. Bustamante).

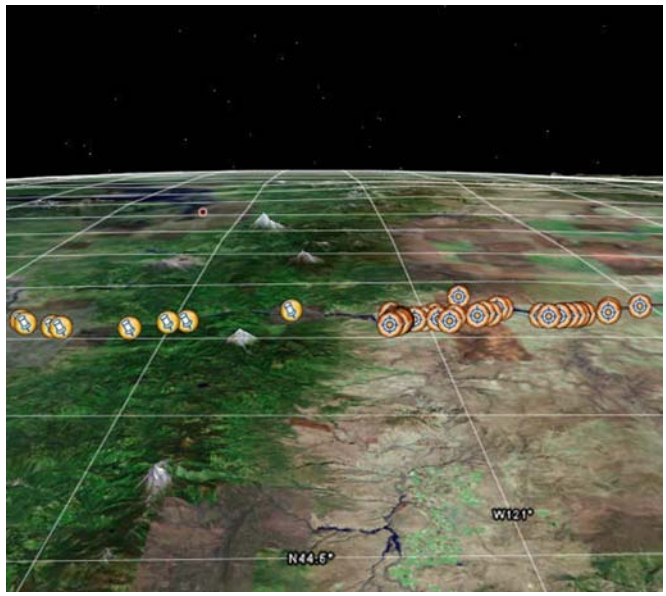

Fig. 40. Columbia River Basin petroglyph sites. Shown is a 45-km elevation oblique view from the south of petroglyph sites on the north bank of the Columbia River (center, 45.7° N, 121.5° W). Mount Hood (south of the Columbia River) and Mount Adams (north of the Columbia River) are shown near center left.

B. Western United States

The western United States is the most heavily surveyed region in this paper (two of the authors, A. L. Peratt and A. H. Qöyawayma have a combined total over 120 years of walking, hiking, hunting, climbing, rafting, four-wheel driving, and bivouacking the west, as well as studying its wildlife, archaeology, history, and peoples).

Because of the amount of data taken over years, we shall concentrate of a few selected sites out of all those shown at the upper left of Fig. 3.

1) Columbia River Gorge: From its Canadian ice fields and glaciers to the Pacific, the Columbia River runs entirely through basalt rock, dropping 380 cm/km, on its 2044-km journey. The middle section of the Columbia runs 674 km between the International Boundary and the Snake River. The lower section then runs west 404 km to the Pacific Ocean. However, like the Lorings before us [23], whose petroglyph-logging efforts are not likely to be exceeded, our surveys have been along a 225-km section between 121.14° W and 120.03° W (Fig. 40).

While several tens of thousands (or more) petroglyphs are underwater (thereby preserved by the slow-moving river) due to the construction of 14 dams on the Columbia River between 1933 and 1984, old topographical maps, site locations, and petroglyph rubbing recorded symbols on cloth exist in library files.

With privatization of waterfront land in the years after the Lorings survey, we have been forced to look in other places adjacent and above the shore line, finding many petroglyphs that the Lorings could afford to pass by (Fig. 41).

A basalt region devoid of petroglyphs noted by the Lorings and ourselves exists where the Cascade Range, between Mount Hood and Mount Adams, crosses the Columbia river (Fig. 40). Here, the terrain to the south increases in elevation on either side of 3400-m elevation Mount Hood, east and west, and the inclination angle at the river rapidly exceeds 40°, blocking the SFOV.

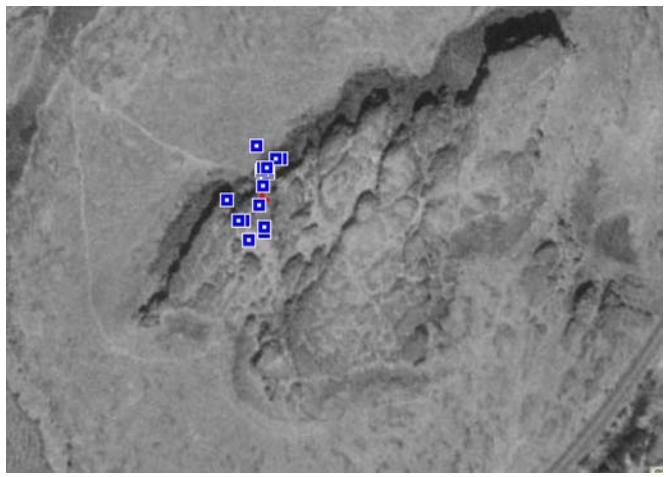

Fig. 41. One-meter-resolution aerial view of petroglyph locations on Horse Thief Butte (45.6° N, 121.0° W), adjacent the Columbia River.

Figs. 41 and 42 illustrate the SFOV of petroglyphs using a 1-m-resolution aerial photograph and compass (for greater accuracy, a tripod and transit are used).

The Columbia River is probably the largest single source of petroglyph data in the western United States.

2) California and Oregon: The California coast region is no longer assessable to a systematic study of pictographs and petroglyphs. The data shown come from logs dating back to the late 1800s.

In contrast, the Oregon coast is not privatized and was accessible to our surveys.

Nearly all of our loggings in California were in Kern, Inyo, and Mono counties, with logging also done in the lower Mojave Desert region. Saline and Death Valley were also logged, as

Fig. 42. Compass orientation in rock gap from Fig. 41. South pointing needle is at top of compass while polar south is midway up the 30° offvertical rock slope on the left. Magnetic declination, 16°49' E; SFOV "skirts" the left or east panel.

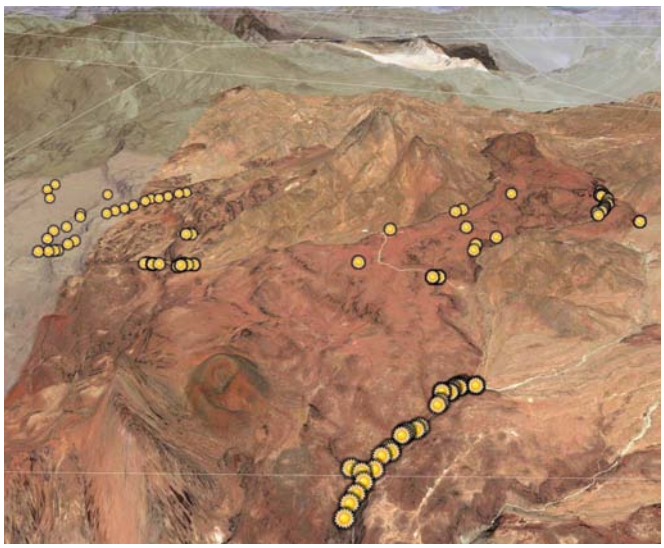

Fig. 43. Coso Range Petroglyphs, with the exception of those on the Columbia River Gorge above and under water, are one of the largest concentrations of petroglyphs in North America. Louisiana Butte is volcanic peak in the upper center of the picture. From the left, are two north–south running canyons: Horse Canyon and Petroglyph Canyon. Sheep Canyon runs from the southerly end of Petroglyph Canyon in a west–east direction with appreciable rock art sights where SFOVs occur in its gullies and slopes. Renegade Canyon is shown at the bottom right of the picture, the rich concentration of engraving ending abruptly where the SFOV is cut off as the canyon enters a gorge (35.98° N, 117.62° W).

were sites further north in the Lake Tahoe and Donner Pass environs.

The low altitude cluster of markers, which is shown in Fig. 43, is the Coso Range on the Naval Air Weapons Station at Ridgecrest, California, another of the world's premier petroglyph locations.

The areas shown are Petroglyph, Horse, Sheep, and Renegade canyons. All sites are oriented so that they are along panels

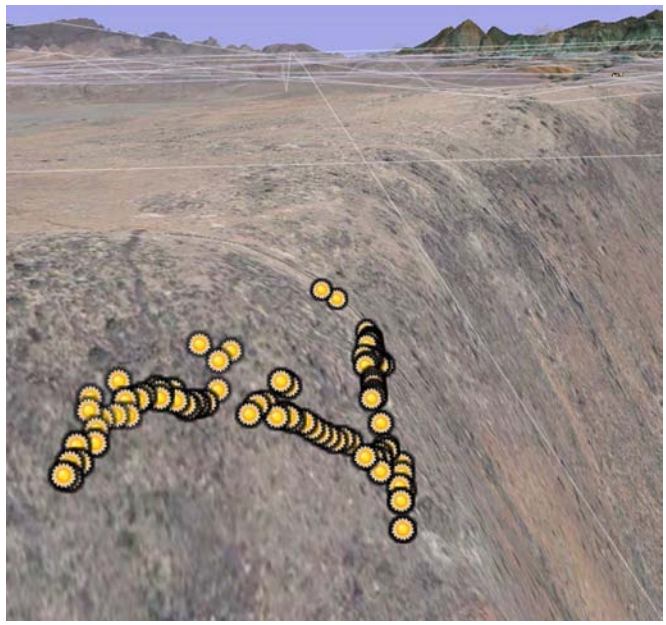

Fig. 44. Central Arizona. SFOV petroglyphs shown at the edge of steep escarpment.

within the canyons or higher up, i.e., all have an SFOV, as did the other sites mentioned in this section.

3) Nevada: Not unlike Death Valley, Nevada, despite its plethora of petroglyphs, can be one of the most uninhabitable of places in the summer. Nevertheless, it is a survey treasure.

Some 45 sites have been surveyed in Nevada, including the Nevada Test Site to which one of the authors (A. L. Peratt) has access. Because of the volume of data taken in Nevada and its extraordinary orientation information, this data will be published elsewhere.

4) Arizona: Arizona, home base for the Tucson Team, has been heavily surveyed. Several sample sites are shown.

Fig. 44, an escarpment in central Arizona in a region of one of the authors home (A. H. Qöyawayma) shows a typical distribution of petroglyphs: carvings on rock with an SFOV, suitable inclination, and blinder (the other side of the canyon). Fig. 45 shows additional data taken near the author's home. These include both pictographs and petroglyphs.

Fig. 46 shows our data of the Petrified Forest National Monument in the vicinity of "Newspaper Rock." The figure shown, for greater accuracy, is that of a 3-D topographical map. The reason for the petroglyph locations on this peninsula-shaped escarpment, with identical basalt-panel escarpments on the west and east sides, is shown on the figure: A higher mountain range shields SFOV in front of the blank areas on the peninsula.

5) New Mexico: The principle high-density petroglyph sites in New Mexico generally lie within the north–south-oriented Rio Grande valley, or in the mountains on either side of it. The greatest number of petroglyphs logged lie in central and northern New Mexico, from Three Rivers in the south to Arsenic Canyon in the Rio Grande Gorge to the north.

Fig. 47 is a layout of Petroglyph National Monument, Albuquerque, New Mexico (35.14° N, 106.73° W). This field contains 33 000 logged petroglyphs, all have an SFOV. The

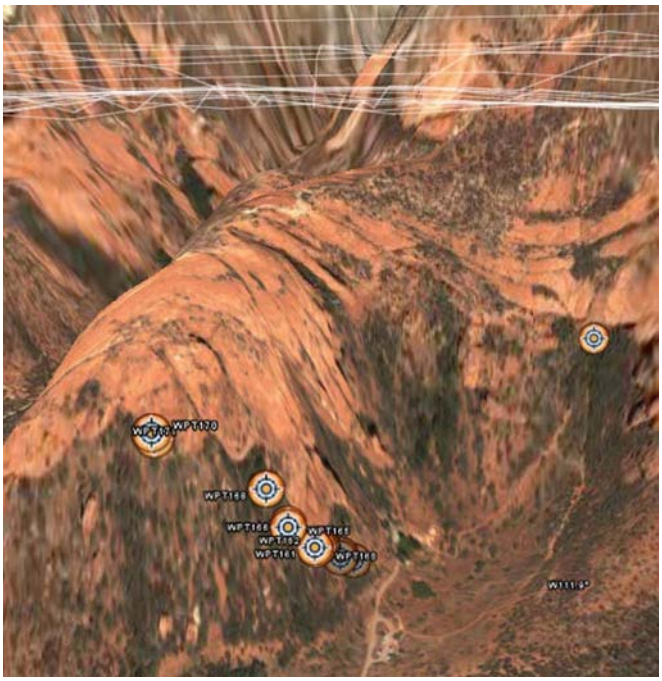

Fig. 45. Hopi Palatkwapi pictograph and petroglyph markers in Central Arizona.

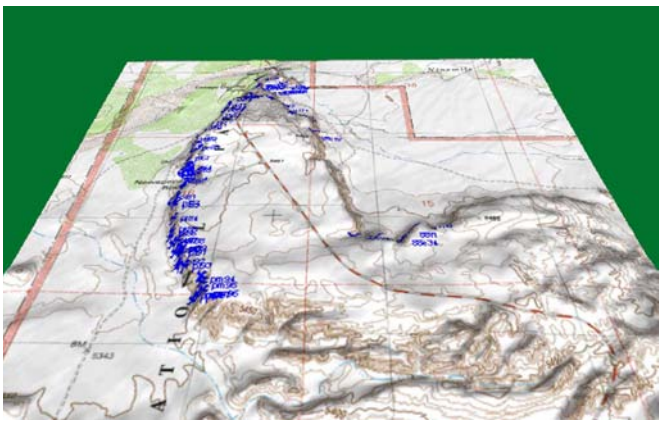

Fig. 46. Petrified Forest National Monument, Arizona. Top: GPS topographic markers at Newspaper Rock site (34.96° N, 109.79° W), center of marked area. The higher altitude mountain range to the south prevents a SFOV beyond the areas marked.

petroglyphs to the northernmost region are on northern slopes but have an inclination less than 27° off-horizontal. Petroglyphs have also been logged with SFOVs on a string of north–south volcanoes shown on the left of the figure.

Fig. 48 is a 2-km-long southeast escarpment with just under 7500 logged petroglyphs. Although the central region has the same basalt panels as the southeast escarpment, the SFOV is lost, and the panels are unmarked. The different colored markers denote different logging dates. Beneath these aerial pictures is a photograph of the escarpment.

Located near one of the author's home (A. L. Peratt), Fig. 49 is a classic example of petroglyphs within a channel. On the left are petroglyph markers at the end of a long SFOV channel in the terrain. The terrain is appreciably steeper than shown in the 6-m-contour separation distance smoothing computer

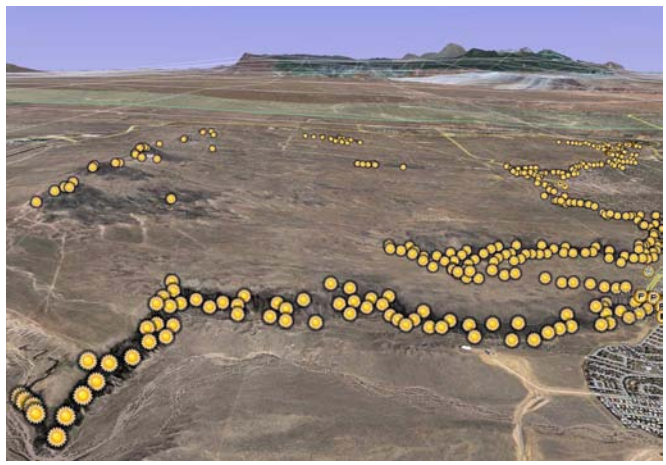

Fig. 47. Petroglyph National Monument, Albuquerque, New Mexico (35.14° N, 106.73° W). This field contains 33 000 logged petroglyphs, all have an SFOV. Upper left: Petroglyphs carved along the north–south-aligned volcanoes. The petroglyphs to the northernmost region are on northern slopes, all with an inclination less than 27° off-horizontal. Bottom: Petroglyphs carved on the south-facing escarpment.

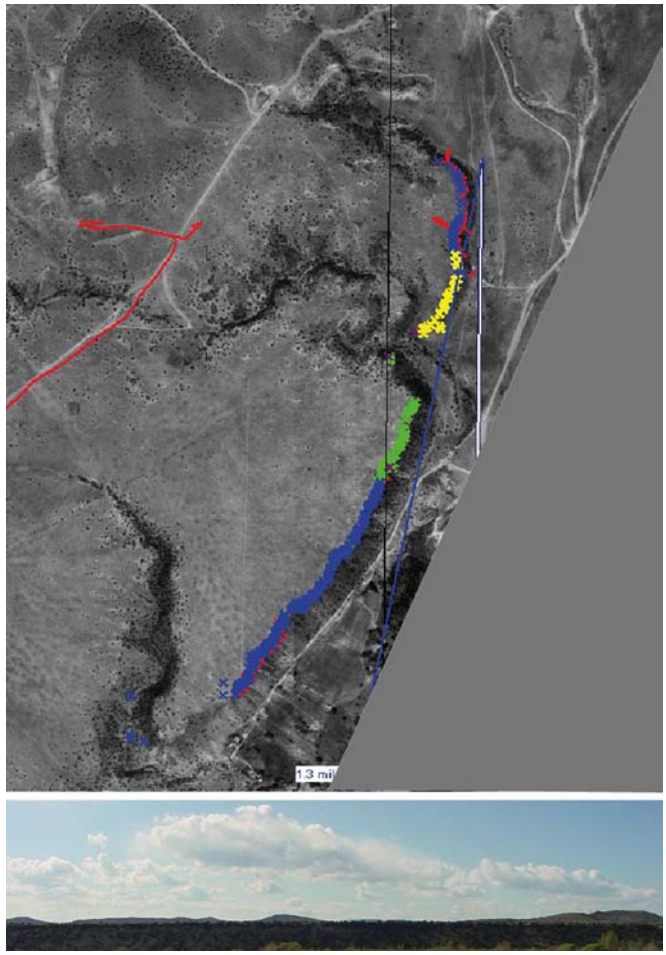

Fig. 48. Top: 3-D view of a 1.8-km-long northeast–southwest escarpment in Northern New Mexico with 7500 logged petroglyphs. Right: 2-D view. The different colored markers denote different logging dates for the petroglyphs running the vertical length of this topograph. Although the central northwest–southeast region has the same basalt panels as the northeast–southwest escarpment, at the bend shown at the center of the topograph, the SFOV is lost and the panels are unmarked. The lines shown on the dirt roads are GPS alignment tracks. Bottom: Partial view of the escarpment to the west.

Fig. 49. Northern New Mexico. Left: Petroglyph markers at the end of a long SFOV channel in the terrain. The terrain is appreciably steeper than shown in the 6-m-contour smoothing computer representation. Right: Center of the picture is oriented polar south. In spite of the narrow radiation channel from the south, the SFOV and inclination is determined locally. For example, the petroglyphs are carved on the northeast side of the boulder where the artist had a peek view of the sheath instabilities while blocking the intense light from the center of the plasma inflow (data recorded by one of the author's, A. L. Peratt, and M. Rowe, Texas A&M).

representation. On the right of Fig. 49 is a photo at the actual petroglyph site. The center of the photo is oriented polar south. In spite of the narrow radiation channel from the south, the SFOV and inclination is determined locally. For example, the petroglyphs are carved on the northeast side of the boulder where the artist had a peek-view of the sheath instabilities of an intense aurora while blocking the bright light from the center of the plasma inflow.

Another type of channel in the vicinity of the site, which is shown in Fig. 50, is that of a 3200-m mountain directly south of a petroglyph escarpment. The petroglyphs are carved either on the east facing or along the top of the escarpment. Other basalt boulders lie on the eastern and western slopes of this geological feature but are void of markings.

The bottom part of Fig. 50 illustrates the uniqueness of this site as viewed from 20 km to the south at an altitude of 13 km. A natural channel formed by the mountain's slopes and contours provides a viewing inclination angle of 27° to 29° (center line), 8° E of polar south, at the escarpment. When the sides of the channel increase to 31° (outside lines), the escarpment is absent of markings.

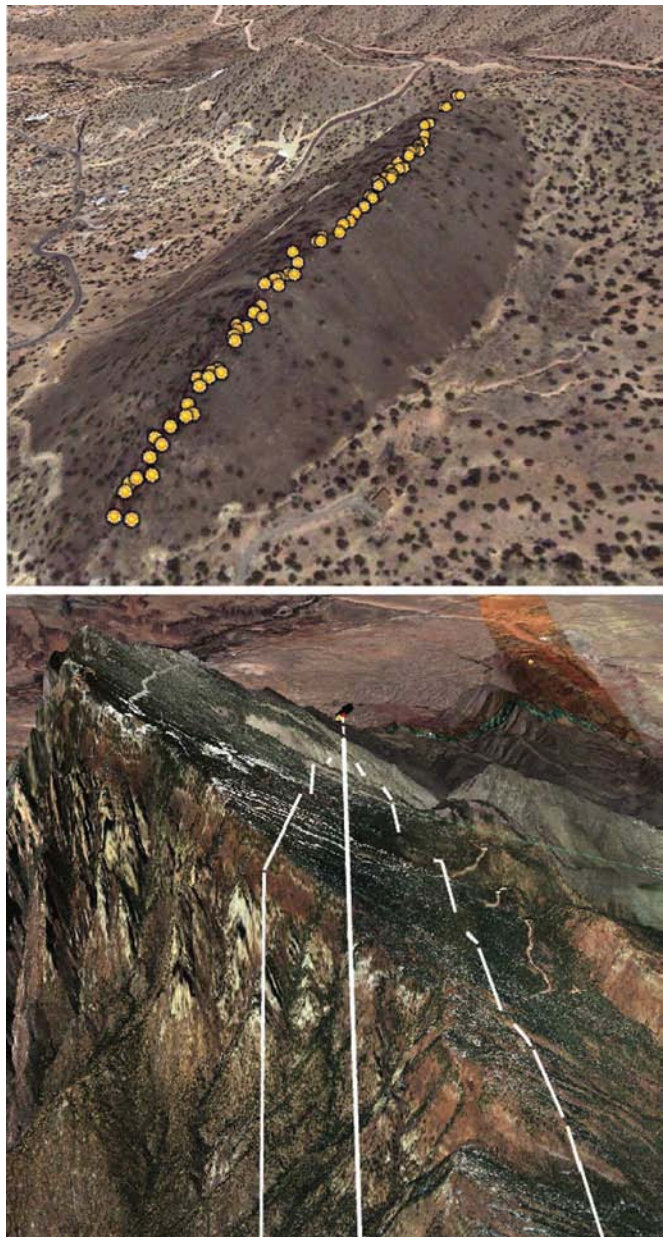

Fig. 50. Top: Petroglyphs along a 1800-m elevation basalt escarpment 20-km true north of a 3200-m elevation mountain. All of the petroglyphs are on the eastern side of the escarpment and, for the most part, absent of any local blinders (Section II-A). Bottom: Oblique view north to the escarpment. A narrow channel formed by slopes and contours of the mountain, shown by the white center line, has an inclination of 27°–29° and runs unimpeded 8° E of polar south. The lines east and west of the channel delineate where the escarpment SFOV inclination has increased to 31°.

XII. Australia

Fig. 6 shows a general distribution of petroglyph sites in Australia.

While some data were obtained for all sites across Australia, the Flinders Range above Spencer Gulf in South Australia was heavily surveyed over a period of six years. The importance of detailed FOVs, transit orientations, and inclinations for this region is due to its far south location, very close to where Birkeland currents entered the upper atmosphere. For this reason, Tasmania and New Zealand were included in this survey.

The surveyed regions include Arkaroo Rock, Arnhem Land, Brisbane, Burra-Karolta, Jabirringgl, Cleland Hills, Deaf Adder Creek, Iga Warta, Malka, Mount Chambers, Mudlapinha Springs, Olary, Ororoo, Penena Creek, Red Gorge, Sharpey's Ridge, Victoria River, Willow Springs, Windjana, Yourambulla, Anthony Hill, Argyll Rock, Ayers Rock, Burra, Farraand, Fitzmaurice-Victoria Rivers, Simulacrum, Uluru (Ayers Rock), Wartylunha, Wilpena Pond, Windjana Cave, Wollemi National Park, Yurlu, and Boehm.

Three examples out of our data set are graphically shown in Figs. 51–53. Fig. 51 marks the sites of the petroglyphs at Yourambulla Caves, Flinders, South Australia. Fig. 52 depicts the petroglyph locations at Red Gorge, while Fig. 53 shows the orientation of petroglyphs in the Mount Chambers environ, all in Flinders. All data have a SFOV.

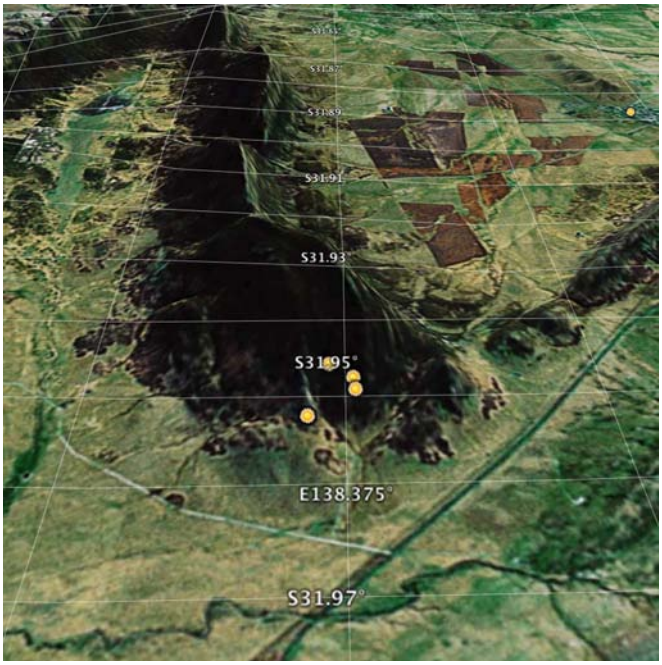

Fig. 51. Yourambulla Caves, Flinders, South Australia (31.95° S, 138.61° E).

Fig. 52. Red Gorge, Flinders, South Australia (30.57° S, 138.61° E).

This voluminous South Australia data set verifies and validates the data collected from elsewhere around the Earth. Because of the large size of this data set, it will be discussed in detail elsewhere.

XIII. Technical Discussion

Petrogyphs, and pictographs only in association with petroglyphs, can have any "facing" (the direction of a normal vector out from the petroglyph; this can be in any direction: north, south, east, west, up, or down, as in the ceilings of caves). It is the FOV of the eye of the working artist that

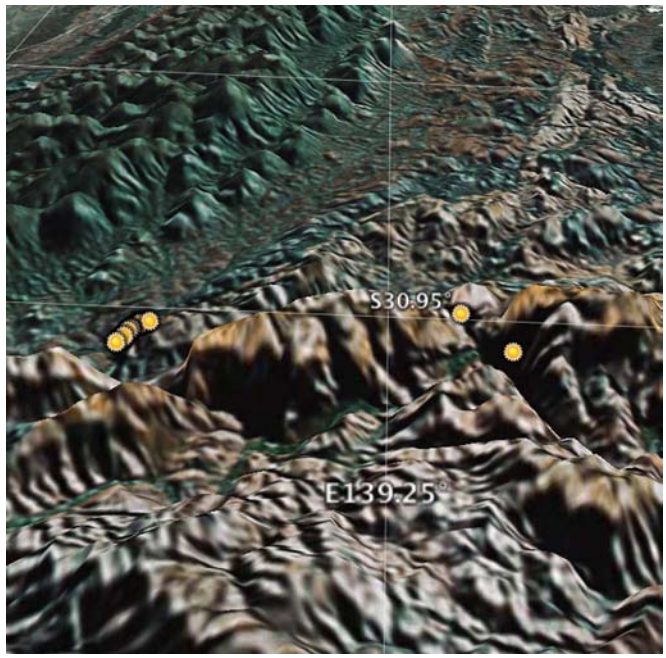

Fig. 53. Mt. Chambers Gorge, South Australia (30.57° S, 138.61° E). The voluminous amount of data taken in the Flinders Range that will be published elsewhere.

determines the inclination and directionality recorded at any petroglyph location. This may be considerably different and far more limited than the "facing." Pictographs in caves have no FOV [4].

Petroglyphs carved at the top of a hill or peak may provide a $0°-360°$ FOV, only one direction that the artist was sighting, while the facings (Section II-A) may be in any direction. Well-drawn concentrics are often found in greater numbers at these locations, or high up on an escarpment.

Petroglyphs carved on the north side of a slope occupy an increasingly narrower portion of the compass with a FOV centered on $180°$ south as the distance from the peak increases. A null (void of markings) region is reached at an inclination of $+24°-+31°$ downward from the peak whose location at which the artist used local blinders. This description is also applicable to petroglyphs carved on the east, west, or south slopes downwards from the peak.

Of the sites surveyed, an estimated four million petroglphs, only one exception has been found. This was on a boulder adjacent a trail to a mountain village in Valcamonica that lay in a small valley with no appreciable FOV. The petroglyph itself was indiscernible but may have been a Christian cross.

In the northern hemisphere, all petroglyphs are oriented with an SFOV, some of which are located far back in caves, crevices, confined mountain passes, or along rivers with canyon- or forest-limited FOVs, having only a polar south view with a variation of a few degrees. In these locations, no FOV in any other direction other than south has been recorded.

In South Australia, a bend in the plasma column far above the Earth was noted. Nearly normal to Antarctica, the column bends eastwards as seen from Australia and presents an increasingly "stretched" columnar profile for New Zealand and more so for South Africa (Fig. 1).

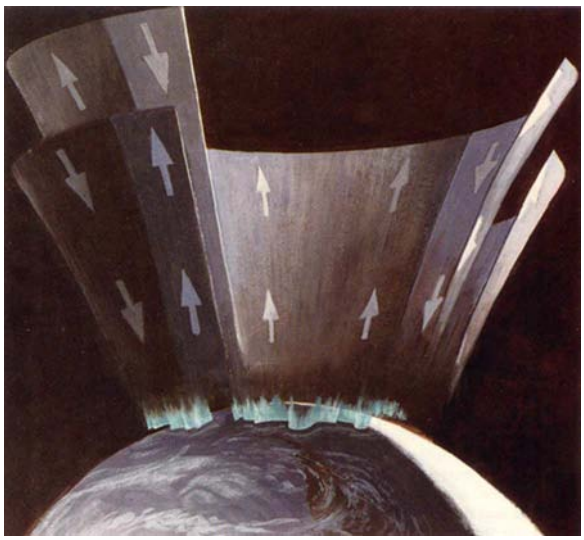

Fig. 54. Artists depiction of Birkeland currents flowing in and out of the Earth's atmosphere at high latitude. These currents, once the subject of intense debate, are routinely measured by today's satellites and have total magnitudes of millions of amperes (mega-amperes) (courtesy of S. G. Smith, Applied Physics Laboratory, The Johns Hopkins University).

Fig. 55. Space-shuttle image of the aurora illustrating the auroral curtains colors, red at top, greenish-white at bottom, with altitude above the Earth (courtesy of NASA archives).

This bend allows much of the column and plasmoids [6] in our model to be seen at the equator and both northern and southern latitudes.

The view from Tasmania, The Tasmanian Paradox or "why are the petroglyphs so dominated by circles," is due to a geometry of FOV up into a concentric column.

This topic is discussed in greater detail in Section XVI.

XIV. Reconstruction of a Virtual Image of the Intense-Aurora Z-Pinch

A. Properties of an Aurora

The shapes of contemporary aurora are determined by the supersonic solar wind, Earth's magnetosphere, magnetospheric shields (approximately 100 km above the Earth's surface) at about 10 R_E (Earth radii), and Earth's dipolar magnetic field. It is the magnetopause that diverts the impinging solar wind into a tear-dropped-shaped shell and extended magnetoshell.

At the widest, the width of the magnetosphere is approximately 100 000–150 000 km while the tail stretches away from the Earth for 1 000 000 km or more (for comparison, the mean distance between the Earth and the Moon is 384 402 km).

The circular or oval in-flowing and out-flowing electrical currents are shown in Fig. 54. These sheets of electrical currents form the rapid waving curtains of light in an auroral display (Fig. 55), a result of the electrons interacting with and exciting molecules in the upper atmosphere [25]–[27]. The aurora is sporadic, usually lasting for a maximum of several hours, but sometimes for days. The most intense and largest auroral displays occur during a solar storm when the incoming flux increases dramatically [28].

The solar wind deriving from the Sun's 10^6 degree coronal plasma impacts the sunward side of Earth's magnetosphere at a velocity that normally varies from 250 to more than 800 km/s. The density is normally about 10 cm^{-3} with a field strength of 5×10^{-5} G. In contrast, the particle density of the Earth's atmosphere at sea level is about 3×10^{19} cm^{-3}, and the Earth's magnetic-field strength at the poles is 0.6 G.

Despite the dilute nature of the solar-wind plasma and weakness of the interplanetary magnetic field, the flow of solar plasma determines the overall shape of Earth's magnetosphere. The flow of electrons and ions into the Earth's lower ionosphere region along magnetic fields at the north and south polar openings (polar cusps) are called Birkeland currents [29], [30].

When an intense coronal mass ejection occurs ($10^{17}g$, 400–1000 km/s) near the center of the solar disk and its magnetic field is strong and oriented southward, the power of the solar-wind–magnetosphere generator may exceed 10 TW. Simultaneously, the magnetic field produced by the auroral discharge current produces an intense geomagnetic storm ultimately heating Earth's upper atmosphere. When oxygen atoms collide with heated atoms, the atoms emit a dark red light (the "red glow") seen high in the aurora curtain, generally 250–1000 km in altitude (Fig. 55).

Between 100 and 250 km, the auroral curtain is greenish-white in color at a wavelength of 5577 Å emitted from atomic oxygen (O) subjected to 6-keV electrons.

One of the basic forms of the aurora is a curtainlike structure that is generally referred to as an auroral arc. When they appear in multiples, their typical separation distance is 30–50 km. Each arc consists of several arc elements, which have curtainlike structure; the thickness is a few hundred meters and the typical separation distances are a few kilometers. The curtainlike form of the aurora exhibits deformations known as curls, folds, and spirals. Spirals that occur, when the Birkeland current peaks, are 50 km in size, have a lifetime on the order of 10 min, and have a clockwise rotational sense. These auroral morphologies are a consequence of the diocotron instability [6].

While the aurora borealis and aurora australis are nearly mirror conjugates in appearance, the various mechanisms

that control bipolar regional differences and commonalities in electrodynamics of the Earth's magnetosphere–ionosphere–thermosphere system are not well understood. Thus, the aeronomy of the upper atmosphere over the Arctic and Antarctic is a topic of ongoing study [31].

B. Laboratory and Simulation Studies of Aurora Curtains

One of the outstanding problems in the propagation of electron beams along an axial magnetic field is the breakup of the beam into discrete vortexlike current bundles when a threshold determined by either the beam current or distance of propagation is surpassed [32]–[35]. The phenomena, when observed closely, resemble that associated with the Kelvin–Helmholz fluid dynamical shear instability, in which vortices develop throughout a fluid when a critical velocity in the flow is exceeded, with a large increase in the resistance to flow [4].

While structural changes in the azimuthal direction are observed in solid, annular, or sheet beams, it is with thin-sheath hollow electron beams that the vortexing phenomenon is most pronounced. Thin-plasma hollow beams are easily produced and are capable of conducting currents exceeding those given by the characteristic Alfvén value [36].

For strong-magnetic-field low-density beams, the cross-field electron-beam parameter is given by

$$q = \omega_{pe}^2/\omega_{ce}^2 \tag{1}$$

where $\omega_{pe}^2 = n_e e^2/m_e\gamma\varepsilon_0$, $\omega_{ce} = eB/m_e\gamma$, $\gamma = (1-\beta^2)^{-1/2}$, and $\beta = v_z/c$ for a beam of axial velocity ν_z. For strong-magnetic-field low-density beams, $q < 1$, and for a beam of thickness Δr, the instability occurs at long wavelengths [33]

$$\lambda \approx (\pi/0.4)\Delta r. \tag{2}$$

The e-folding length for instability buildup is

$$L = \lambda C B_z V/I \tag{3}$$

where C is the beam circumference, B_z is the longitudinal magnetic field, V is the voltage, and I is the current in MKS units. Peratt and Snell [33] have studied the cross-sectional views of hollow beams with conducting currents from 7 μA to 6 MA over 12 orders of magnitude in current. The onset of the diocotron instability satisfying (3) is shown in Fig. 56.

C. Formation of Birkeland Currents in Laboratory Experiments

For distances less than that is given in (3), the filaments are constrained by the generalized Bennett relation [6], or if rotation is ignored, by the Bennett relation

$$\mu_0 I^2/4\pi = 2NkT. \tag{4}$$

Birkeland, using eight cameras and eight screens, was apparently the first to capture the nature of these Bennett-constrained filaments, as shown in Fig. 57. Depicted are currents flowing

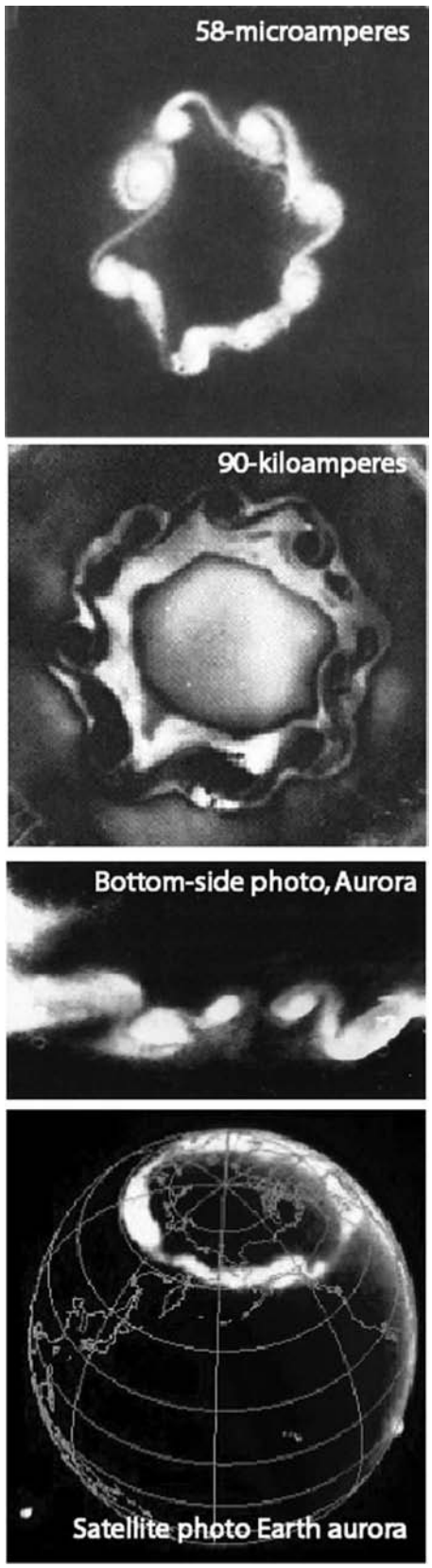

Fig. 56. Frame 1 (top): 58-μA hollow electron beam recorded on a fluorescence screen (courtesy of H. Webster, General Electric). Frame 2: Diocotron instability recorded on a steel witness plate impacted by a hollow 90-kA beam at Los Alamos National Laboratory. Frame 3: Ground view of overhead aurora (approximately 1 MA) from televised frame (courtesy of T. Hallinan). Frame 4: Auroral activity around Arctic on July 15, 2000 (courtesy of NASA/IMAGE far-ultraviolet archive).

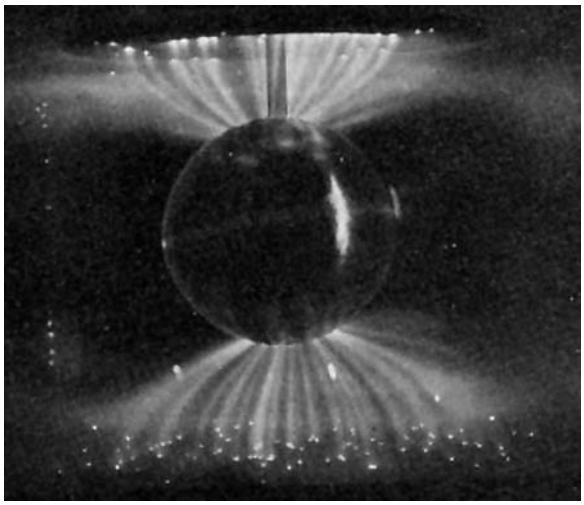

Fig. 57. Birkeland's 8-cm-diameter copper globe with a discharge current of 10–20 mA. The globe is an anode between two cathode plates in a 320-L vacuum chamber containing 0.013–0.012 mm Hg.

from the 8-cm copper anode globe, one of 16 "terrellas" he experimented with, ranging in size from 2- to 70-cm diameter (a terella is a magnetized sphere in a vacuum chamber; electron beams are shot against the sphere; residual gas in the chamber makes the path of the beams visible as they are bent by the magnetic field of the sphere). In his other photographs, the filaments can be seen running along the surface of the globe.

As current was increased to the electromagnet within the globe to simulate the Earth's magnetic dipolar field, the currents were forced toward the poles of the terrella, eventually satisfying (3) to produce "auroral" rings around each pole.

Densitometer scans across the Bennett-constrained currents in his photographs show approximately 56 filaments, many in pairs.

An estimate for the currents in an intense aurora can be obtained from Alfvén and Carlqvist [6, p. 62] who find, for a strong circular aurora of diameter 5000 km, a total current of about 7 MA. If this pertains to 56 filaments (before the ring is formed), each filament conducts 125 kA. Hence, (4) is satisfied, and the currents remain as pinched filaments.

D. Formation of Birkeland Filaments in a 90-kA REB

Fig. 58 shows the pattern of a 90-kA particle beam from a thin circular cathode as recorded on a steel witness plate. The periodicity of the beam filaments (white dots) is 56. For comparison purposes, a circle of 56 evenly spaced outer dots has been superposed onto the witness plate.

E. Dense Plasma Focus (DPF)

The DPF is among the most interesting of high-energy plasma devices. A capacitor bank, or a highly explosive magnetic-compression generator, is discharged through two coaxial electrodes, called a "plasma gun," forming a plasma-current sheath between the inner and outer electrodes. The $j \times B$ force accelerates the sheath outward to the ends of the electrodes where the inner sheath radius is forced inwards toward the center electrode forming a columnar pinch or

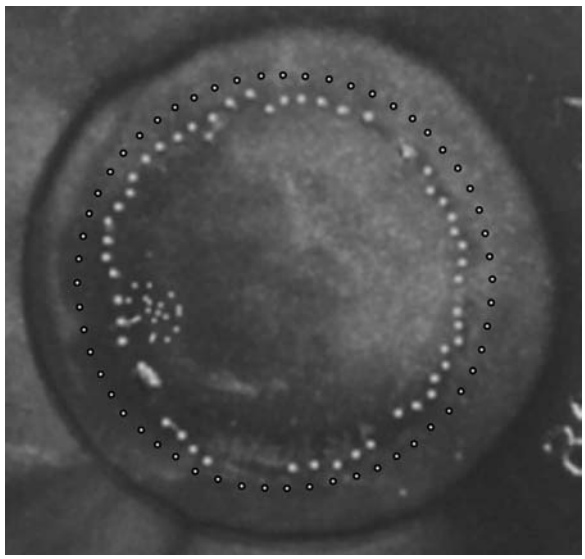

Fig. 58. Pattern of a 90-kA particle beam from a thin circular cathode as recorded on a steel witness plate. The periodicity of the beam filaments (white dots) is 56.

"focus" on axis. The outer sheath, the "penumbra," is a chalice of current filaments [6]. The inner electrode is usually the anode, as was Birkeland's copper terrella.

According to Haines [37]: "Many of the earliest experiments in controlled thermonuclear fusion research were Z-pinches. However, they were found to be highly unstable to the $m = 0$ (sausage) and the $m = 1$ (kink) MHD instabilities, and to the $m = 0$ Rayleigh–Taylor instability. ... Meanwhile studies of the plasma focus, which after its 3-D compression closely resembles a Z-pinch, have shown that a plasma of density 10^{25} m^{-3} and an electron temperature of 1 keV can be achieved in a narrow filament a few millimeters in diameter and about a centimeter in length. It sometimes can have enhanced stability properties which might be attributable to the effect of the finite ion Larmor radius."

With regard to the DPF, the usual number of filaments formed in the penumbra or "chalice" at the pinch is either 56 or 56 paired filaments. Fig. 59 shows the penumbra created at pinch in a 174-kA discharge-current DPF. The periodicity of this chalice structure is 56. Fig. 60 shows the penumbra created at pinch in a 1.8-MA discharge-current DPF. At this higher current, 56 pairs of filaments are discernable in the open-shutter photograph. The figure to the right is an overlay of 56 lines on top of each filament pair. Milanese and Moroso [38], using a low-power 250-kA DPF, report "about 60" filaments recorded by their image converter camera in a series of experiments.

F. Evolution of Plasma Filaments via the Biot–Savart Force

In its simplest, the Biot–Savart Force law states that current filaments or wires running in the same direction attract, while those in opposite directions repulse. For plasmas, instead of wires, there is a neutral force region where the filaments do not merge but rather start a rotational motion around each other to form a vortexlike geometry. In the laboratory, this is most often seen for the closest pairs of filaments but also for three filaments [6].

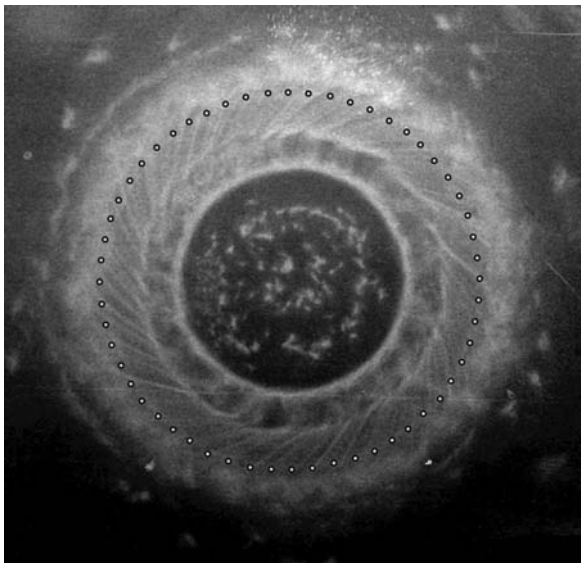

Fig. 59. Penumbra of a DPF from a discharge current of 174 kA. The rotational structure has a periodicity of 56 as shown by the 56-dot overlay pattern.

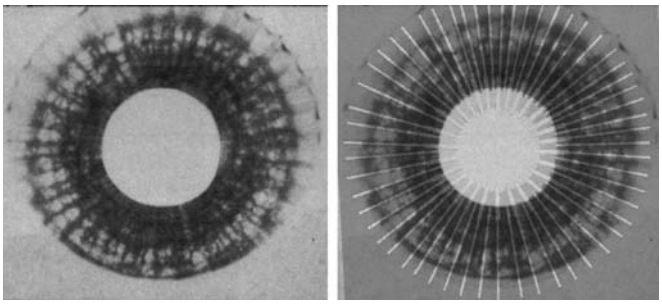

Fig. 60. Penumbra of a 1.8-MA DPF with 56 pairs of filaments as shown by the 56-rayed pattern overlay.

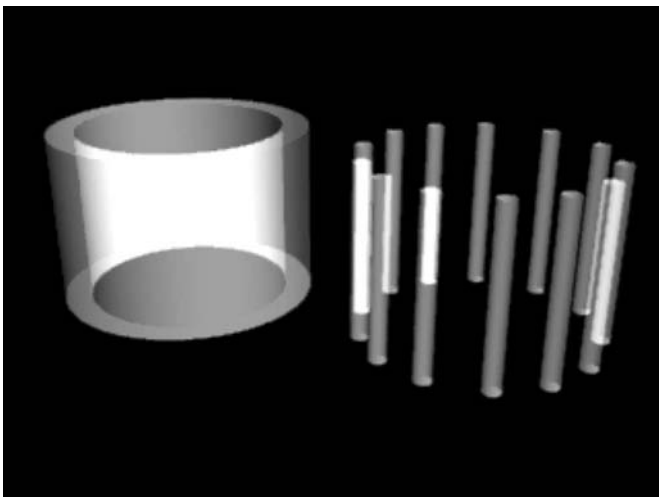

Fig. 61. Basic characteristic of a very thin plasma sheath of relativistic electrons and ions flowing along a longitudinal (vertical) magnetic field; the sheath filaments into 56 current filaments.

Fig. 61 is an artist's illustration of a hollow relativistic charged-particle beam forming individual current filaments. Fig. 62 (top) shows a particle-in-cell simulation of two currents merging to form one thicker filament. Fig 62 (bottom) illustrates the merging of adjacent filaments, starting with 56, to end up with four.

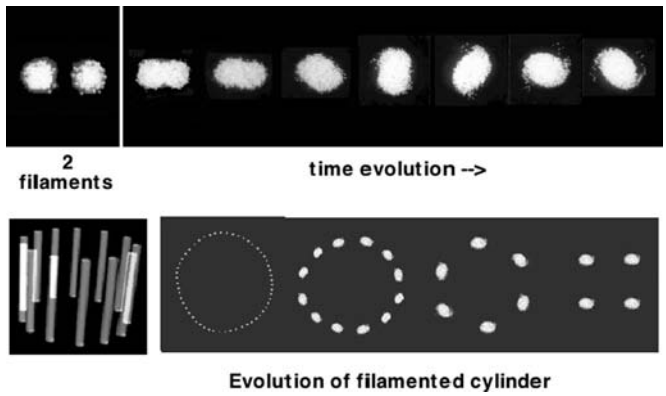

Fig. 62. Top: Particle-in-cell time evolution of two adjacent filaments, as shown by the cross sections of the plasma. Two, and sometimes three, filaments are drawn together to form a vortex structure. Bottom: Rendition of 56 filaments converging to four currents during current increase.

The most common pairing or tripling, as determined from petroglyph surveys, is 56 (by far the most common), 49, 47, 41, 39, 33, 30, followed by a large number of 28-ray petroglyphs and other structures. The converging continues through 20, 16, 8, 7, 6, and 4, the latter being the minimum number of Birkeland currents recorded but in great frequency.

As an example, Fig. 63 shows a streak camera recording whereby a group of plasma filaments are open-shutter photographed through a slit aperture focused across the array. In Fig. 63, time increases from top to bottom. At the top, the photograph shows six filaments (one of the six is shielded by a filament in front of it) in Biot–Savart attraction. In addition, seen in the early stages of the filaments are micropinches.

The filaments converge to a strong pinch (center) where they twist into a helix structure before untwisting back into six filaments (bottom).

A framing camera was used to capture the twisting filaments at maximum pinch. The resulting "helix" is shown in Fig. 64. In comparison, a portion of an engraved bone from a site in France, presumably from the Magdalenian culture, is shown in Fig. 64.

XV. Properties of an Intense Aurora

The properties of intense aurora described by Gold [5] appear to be similar to the properties of a column of plasma-conducting giga-amperes of current rather than mega-amperes.

Historical reference suggests that intense aurora differs from concurrent aurora in several aspects. One Chinese account (translated from Sung-Shih) is:

> "Red cloud spreading all over the sky, and among the red bands of white vapor like glossed silk penetrating it. They arose from Tzu-wei, invading the Great Dipper and the Wen-Chang, and then dispersed from the southeast."

"Swords," "spears," "white vapor," "like glossed silk penetrating it," "candles in the sky," were terms used to describe the aurora during an intense-corona outburst (Fig. 65). Certainly, these descriptions do not match what is seen during today's auroras, as depicted in Fig. 56. In the following sections, we

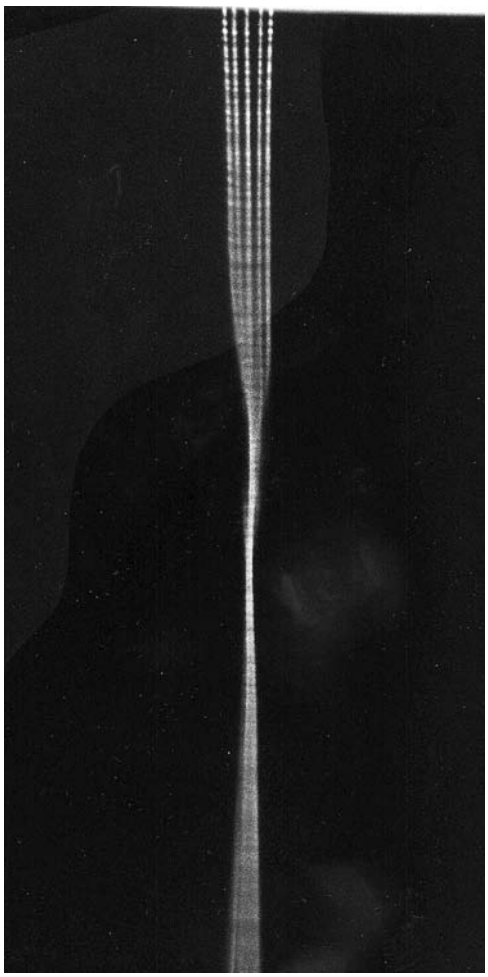

Fig. 63. Streak camera recording with image slit focused across (horizontal direction) six 5-MA current-conducting plasma columns. Time runs from top to bottom, with the columns converging and twisting at the center before separating. Streak photograph by A. L. Peratt, Los Alamos National Laboratory.

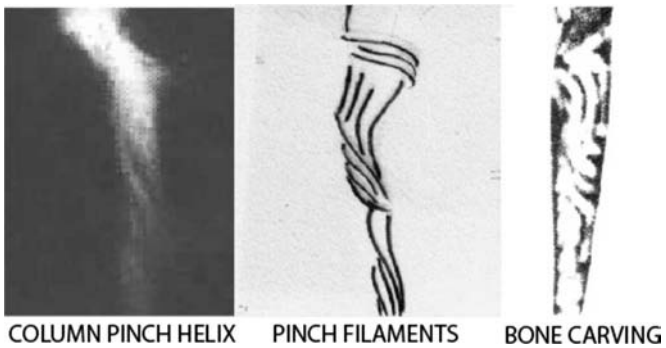

Fig. 64. Left: Single time frame at pinch of six plasma filaments. Center: Helical pattern from line tracing of filaments. Right: Portion of engraved bone from a site in France, presumably from the Magdalenian culture. The section shown is about 1/5 the length of the bone, which is found together with two other bones, display most of the plasma-column instability evolution. Engraved bone photo courtesy of D. Cordova.

investigate the physical effect of increasing the current into the Earth a thousand fold.

A thousand-fold increase of a concurrent aurora is 7 GA, or for 56 filaments, 1.25 MA carried by a filament REB. Estimates will be made for the X-ray fluence and synchrotron luminosity in Part III.

Fig. 65. Red auroras were considered a sign of ill omens during medieval times and pilgrimages were organized to avert the wrath of Heaven. Brilliant displays have frightened people as recently as this century in regions where aurora sightings are rare (courtesy of Zentral Bibliothik, Zurich: from S.-I. Akasofu).

XVI. Observations From the Earth's Surface Within the Sheath

A. Reconstruction of the Plasma Flow During an Intense Aurora

In an intense aurora, the giga-ampere current flow and concomitant strong magnetic field produces a major change in the auroral-height profile. Because of the intense plasma flow and strong longitudinal magnetic field, the plasma forms a thin but dense sheath or plasma column in its propagation toward Earth.

Hence, the in-flowing plasma is a Z-pinch, and as a result, Z-pinch instabilities form as well as intense radiation from the relativistic electrons. The intense radiation consists primarily of X-rays and synchrotron radiation in the visible.

As shown in Part I [6], the synchrotron radiation is that of well-known Z-pinch instabilities in the plasma column. Mankind in antiquity accurately recorded this colorful display of bright lights in many ways. Here, we shall concentrate on the petroglyph and pictograph data recorded worldwide from fields containing about four million markings. Unexpectedly, of those petroglyphs accurately surveyed and GPS logged, it was found that the light was observed totally from the direction of the south axial pole of Earth.

With the utilization of a large computer, several thousands of surveyed data points were used to map the plasma column. Each petroglyph can be viewed as a "fixed" observatory with a local FOV and carved image in perspective (petroglyphs have no meaning if moved). Each of these "pixels" was then processed using plasma holography techniques for recording laboratory Z-pinches to reconstruct a virtual image.

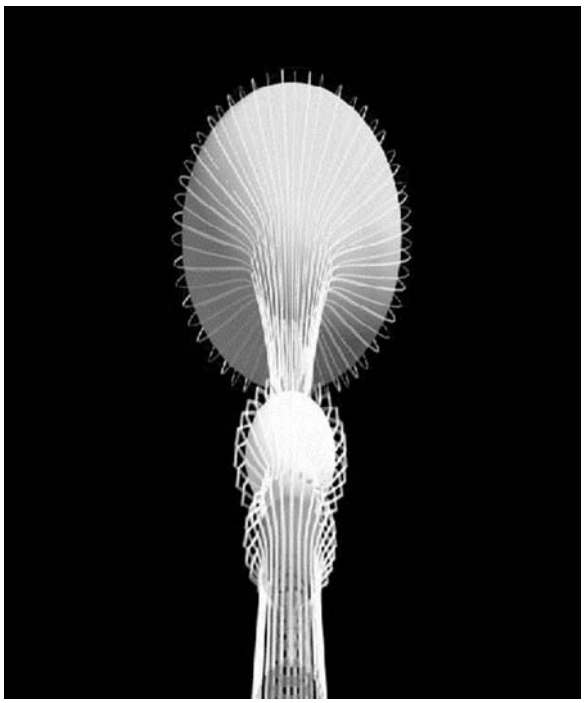

Fig. 66. Virtual image of the intense auroral plasma column as determined from FOV directivity, viewing angle of inclination, and GPS surveys of worldwide petroglyph "pixels." Not to scale.

B. Virtual Intense Aurora Image

Fig. 66 is a virtual image of the intense auroral plasma column as determined from FOV directivity, angle of inclination, and GPS surveys of several thousands petroglyph "pixels." Two egg-shaped plasmoids are found at 306 000 and 266 000 km, respectively The farthest limit of the reconstruction (top) is located 701 000 km from Earth. The number of Birkeland currents is 56 at the top, converging to 28 at the plasmoids and eventually converging and twisting into four large filaments. If the current oscillates or is sporadic [36, p. 34], the four can separate back to 56 filaments. Whether 56 or 4, or some number in-between, the filaments flow over and past the rotating Earth.

While Fig. 66 shows the column extending normally to Antarctica, in progress is a higher resolution image showing the easterly curving of the auroral plasma column.

XVII. Earth Within a Filamentary Birkeland Current Sheath or "Cage"

The first indication that 56 filaments would form in Earth's space environment came from Birkeland's original terrella experiments (Fig. 57).

The configuration for an intense aurora is shown in Fig. 67, where 56 current filaments of relativistic electrons coming in toward Earth's south pole surround the planet. A complete closed-circuit description is found in [36].

A. Observations from the Northern Hemisphere

As an example, we start with petroglyph pictures from the Columbia River Basin (Figs. 2 and 40), 45.7° N, 121.5° W.

Fig. 67. Conceptual view of the Birkeland sheath filaments surrounding Earth (28 close pairs). The relativistic electron flow is downwards toward Antarctica. As shown in Figs. 63 and 64, the current bundle above Antarctica twists in counter-clockwise rotation. By convention, the Birkeland currents and ion flow is upwards toward the Arctic. Not yet completely resolved is a bend in the upper filament sheath that allows the upper plasmoids and column to be seen at northern latitudes.

Two are shown in Fig. 68, left. These are typical of uncounted numbers of "ray," "spoke," "feather," "hair," and "whisker" petroglyphs recorded worldwide. These pictures may be compared to an image that would be recorded looking slightly obliquely up the current column shown in Fig. 66.

B. Observations from the Southern Hemisphere

1) South America: Fig. 69 is a photo of a vase uncovered at Nasca (Nazca), latitude 14° S, with virtually the same image as the petroglyph (Fig. 68, top-left) carved at latitude 46° N.

In South America, flat terrain and mesas are sometimes marked by kilometer-long, man-made lines. Most of these cross each other at various angles and others start or end with trapezoidal profiles. Construction techniques involve the up-turning of large amounts of patinated pebbles to show the light colored ground beneath or in areas covered by flat heavily

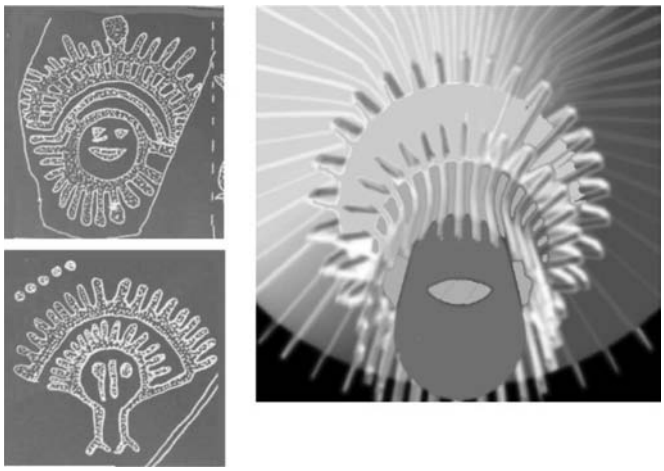

Fig. 68. Left: Northern hemisphere petroglyphs from the Columbia River Basin, 45.65° N, 121.95° W. Right: Oblique view into the auroral plasma column from these coordinates.

Fig. 69. Nasca, Peru vase, date unknown (14.24° S, 75.58° W). Note the similarity to the northern hemisphere petroglyphs (Fig. 68, left).

patinated stones (pavement), flipping the stones to place the whitish under-layer on top—a technique also common to the American southwest.

Markings such as these are found among the Lluta Valley geoglyphs near Arica, Chile, many parts of Brazil, in northern Venezuela, and other regions on Earth. The best known cases are the lines and geoglyphs at Palpa and Nasca, south of Ica, Peru (14.7° S, 75.1° W) ("geoglyphs," a word derived from Greek $ge\bar{e}$ = "Earth, ground" and glyph$\bar{o}$ = "carve, cut out, engrave." Thus, literally, "geoglyph" means "ground carving," although "carving" is not always literally correct where mankind cut through deserts, forests, and mountain ranges to keep the lines as straight as seen from above). What makes the Peruvian lines unique is the sudden flaring of a straight line into a trapezoid geometry.

Fig. 70. Top: Aerial survey of the extent of geometric lines and geoglyphs in the Palpa–Nasca basin. Bottom: Oblique view of the survey makers from the coast, 70–80-km south of the lines.

Fig. 70 (top) plots our aerial survey of the Palpa–Nasca lines and geoglyphs (350–500-m ground altitude), extending 38 km on the flat (450 km^2) desert plains and mesas.

Within the region containing the lines, the SFOV has a high-ground (blinder) gap with elevations of 700–1000 m, 30–47 km to the south, respectively. The range defining the gap rises abruptly to 1700 m at the westernmost boundary of the lines, while the easternmost lines end where the plains meet east–west hills (and a 1600-m mountain range to the south). Fig. 70 (bottom) shows the lines with the SFOV gap, profiled against the high northern mountains.

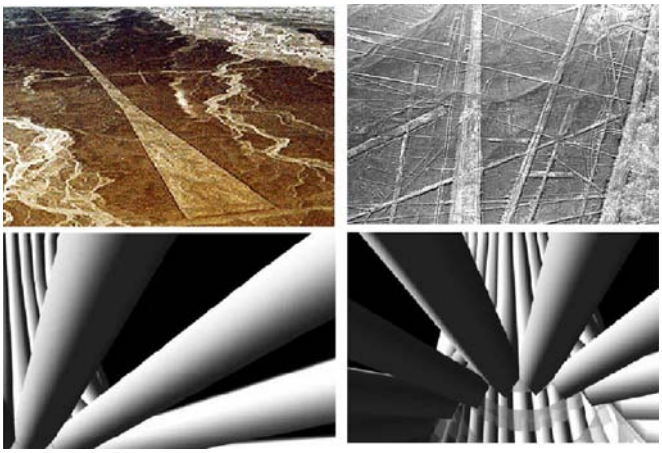

Fig. 71. Top: Trapezoids and lines of the Palpa and Nasca plains. Bottom: View upwards into Fig. 67 from a "camera" placed at the surface of the digital Earth at latitude/longitude 14.24° S, 75.58° W. The historical terms "swords," "spears," "white vapor," "like glossed silk penetrating it," and "candles in the sky," appear appropriate to these pictures.

Fig. 72. White-striped pictographs at Iga Warta Cultural Tourism Centre, North Flinders Range (30.59° S, 138.94° E). Shown is Cliff Coulthard, Australian Department of Environment and Planning in Aboriginal Heritage, an authority on pictograph painting techniques having analyzed such works as the Magdalenian cave art in France.

The characteristics of the Nasca–Palpa lines and geoglyphs differ in no way from the parameters determined for petroglyph locations worldwide.

Fig. 71 top shows pictures of the lines at Palpa–Nasca. If we place a "camera" on the surface of the globe within Fig. 67 at the latitude of the Peruvian lines, 14.24° S, the resulting image is that shown in Fig. 71, bottom. The historical terms "swords," "spears," "white vapor," "like glossed silk penetrating it," and "candles in the sky," appear apropos. Highly focused sharp-edged synchrotron light from the relativistic mega-ampere electrons would have produced white-light images of the filaments on the ground visible even in daylight [4, Sec. 4-B].

Vertical striped petroglyphs or vertical white-striped pictographs are found worldwide. For example, white-striped pictographs are common to Australia, from the Northern Territory to the Flinders Range. One example is given in Fig. 72, Iga Warta, at 31° S latitude.

Fig. 73. Lightning Brothers, Ingaladdi, Victoria River, Wardaman country of the Northern Territory (15° S, 130° E). New dating techniques of this red inorganic-pigmented pictograph image were done using a plasma–chemical extraction method.

One of the better known pictographs, occurring often in Aborigine mythology, are the striped "Lightning Brothers," latitude 15° S (Fig. 73), which can be replicated by looking nearly straight into the plasma columns shown in Fig. 68, right, with the Birkeland currents incoming toward Antarctica making up the torsos of the figures. The dark stripe running vertically in the figures, toward the "nose," is the dense central region of the plasma column.

We refer the reader to Section XV on how mankind in antiquity interpreted these figures.

XVIII. Discussion and Conclusion

That mankind in antiquity did witness and record the effects and images from an intense solar outburst lasting many years can be deduced by the records that have endured, for the most part very little changed, over the millennia [39]–[42].

With the advent of high-energy-density Z-pinches and associated diagnostics, high-resolution high-fidelity three-spatial-dimension electromagnetic particle-in-cell simulations on terahertz computers, and the development of global instrumentation systems, facilities, and instrumentation over the past decade, it has become possible to perform the physics and observations necessary to support suggestions that an intense solar outburst and its effects were observed by mankind in the past.

That the outbursts were extreme is witnessed by the carving on rock of MHD images on rock worldwide, not unlike the eyewitness accounts of "a thousand fantastic figures, as if

painted with fire on a black background" from the September 1859 solar storm [43], less energetic than that discussed in this paper.

The so-called "rib-cage" structures most often found in petroglyphs are a distinct signature of self-similar skeletal structures identified in space plasmas [44]. These petroglyphs are often interpreted as actual objects of anthropological significance relating to cultural behaviors worldwide.

The meaning and creation of petroglyphs in standard accounts, i.e., anthropological, trance metaphors, symbolism, histories, and religions, are not expected to have any correlation with a preferred FOV or astrometric factors as proposed here. One of the authors (A. H. Qöyawayma) notes that "Shaman" is a term not used among the Hopi and is unaware if this concept has any relation to petroglyphs in other Native American cultures. Another of the authors (J. McGovern) recalls the words of the anthropologist C. P. Mountford when visiting Red Gorge, South Australia, for the first time in 1937: "To my surprise, the aborigines did not recognize those rock engravings as human handiwork, even though they must have passed through that gorge many times on their hunting journeys." This suggested to him that petroglyphs were a long-forgotten art [45].

Even in our space-plasma account, one might expect plasma columns under very intense geomagnetic-storm conditions to occur near both magnetic poles just as contemporary aurora occur at both poles for comparatively modest storm conditions. However, we find that petroglyph distributions have no north FOV preference (Section XIII). Standard accounts should be independent of such orientation factors except for the sun angle that affects lighting on available rock surfaces. Moreover, lighting from the Sun would have to explain the SFOV in both the northern and southern hemispheres.

Furthermore, "blinders" (Section II-A) should have no correlation with petroglyph distributions nor should an "angle of inclination." Indeed, as shown in Section XVI, preliminary analysis indicates that the worldwide petroglyph distribution and FOV data enable us to reconstruct the intense plasma column that our model predicts for very intense magnetic storms that occur over the millennia. In a later paper, we will carry out more detailed reconstruction and plasma modeling and show how very intense auroral events were recorded by methods other than carving petroglyphs.

ACKNOWLEDGMENT

The authors would like to thank the Mainwaring Archive Foundation, Bryn Mawr, Pennsylvania, in association with the Museum of Archaeology and Anthropology, University of Pennsylvania, for supporting this research, and to the United States, Department of Energy, National Nuclear Security Agency, for allowing access to energy sources of magnitude equal to that of an intense aurora and the computer facilities necessary to model it. They would also like to thank those who contributed data and/or recommendations for this paper, in particular: A. Acheson, M. Acheson, A. Bodin (LANL), C. Brown (Library of Congress), E. J. Bond, P. Bustamante (Taller Taucan, Chile), D. Cardona, E. Cochrane, D. Comstock (LANL), F. Costanzo (Ariz.), L. Crumpler (NASA), Z. Dahlen, H. Davis (LANL), A. de Grazia (U. Bergamo), A. J. Dessler (U. Ariz.), T. E. Eastman (Perot Systems), I. Eastvold (SFCC), J. Goodman, P. Hedlund, G. Heiken (Geo, LANL), L. Hessink (GWSA), G. Hidy (DRI, EPRI), D. Jensen, H. Johnson, J. Kamm (LANL), K. Kintner (LANL), J. Lawson (NAVAIR, NAWCWD), B. G. Low, A. S. McEwen, M. Medrano (PNM), F. Minshall (USNPS), M. Minshall, M. Mitchell, E. Moffat (Zanskar Survey), B. Moore, J. Nelson (BLM), A. Neuber, S. Parsons, C. Patenaude (equinox-proj.), C. M. Pedersen (Columbia Survey), G. G. Peratt (U. Ariz.), G. Pfeufer (LANL), C. J. Ransom (Vemasat), M. W. Rowe (Texas A&M), T. Scheber (LANL), R. Schmidt (equinox-proj.), A. Scott, D. E. Scott (U. Mass), D. Scudder (LANL), J. Shlacter (LANL), P. Shoaf (NAVAIR, NAWCWD), R. M. Smith (JPL), C. Snell (LANL), D. Talbott, W.Thornhill, H. Tresman, I. Tresman, T. Van Flandern (NRL), T. Voss, W. S-Y. Wang (U. Hong Kong), R. Webb, B. Whitley (Ariz. Petroglyph Steward), P. Whitley (Ariz. Petroglyph Steward), W. Wolfe (W. Aus), F. Yao (APS), and E. Younkin (Curator, Maturango Museum). They would also like to thank the Hopi and Navajo Nations in Arizona and the Cochiti, San Juan (O'ke), Santa Clara, Jemez, Santo Domingo, and San Ildefonso Pueblos in Northern New Mexico for their support. The Library of Congress, The University of New Mexico, Arizona State University, Arizona State Historic Preservation Office, and the Bancroft Library of the University of California, Berkeley, provided access to valuable logs, journals, maps, and topographical information from previous expeditions.

REFERENCES

[1] A. L. Peratt, "Stonehenge—A giant petroglyph?" *Univ. Pennsylvania Almanac*, vol. 48, no. 8, Oct. 2001.

[2] A. L. Peratt, "Evidence for an intense aurora recorded in antiquity," in *Proc. IEEE Int. Conf. Plasma Sci. Conf. Rec.*, Jeju, Korea, Jun. 2003, p. 143.

[3] D. A. Scott and A. L. Peratt, "The origin of petroglyphs—Recordings of a catastrophic aurora in human prehistory?" in *Proc. IEEE Int. Conf. Plasma Sci., Conf. Rec.*, Jeju, Korea, Jun. 2003, p.143.

[4] A. L. Peratt, "Characteristics for the occurrence of a high-current Z-pinch aurora as recorded in antiquity," *IEEE Trans. Plasma Sci.*, vol. 31, no. 6, pp. 1192–1214, Dec. 2003.

[5] T. Gold, "Large solar outburst in the past," *Pontificiae Academiae Scientiarvm Scripta Varia*, vol. 25, pp. 159–174, 1962.

[6] A. L. Peratt, *Physics of the Plasma Universe*. New York: Springer-Verlag, 1992.

[7] H. F. Webster and T. J. Hallinan, "Instabilities in charge sheets and current sheets and their possible occurrence in the aurora," *Radio Sci.*, vol. 8, no. 5, pp. 475–482, May 1973.

[8] A. L. Peratt, "Orientation of intense Z-pinch instabilities from an intense aurora as recorded in antiquity: Western USA," in *Proc. IEEE Int. Conf. Plasma Sci., Conf. Rec.*, Baltimore, MD, Jun. 2004, p. 426.

[9] D. A. Scott and A. L. Peratt, "Orientation of Z-pinch instabilities from an intense aurora as recorded in antiquity: South America," in *Proc. IEEE Int. Conf. Plasma Sci., Conf. Rec.*, Baltimore, MD, Jun. 2004, p. 427.

[10] A. L. Peratt, D. A. Scott, and M. A. van der Sluijs, "Orientation of intense Z-pinch instabilities from an intense aurora as recorded in prehistory," in *Proc. Bull. Amer. Phys. Soc., 46th Annu. Meeting Division Plasma Phys.*, Savannah, GA, 2004.

[11] A. L. Peratt, "Synchrotron radiation from an intense auroral Z-pinch recorded in prehistory," in *Proc. IEEE Conf. Rec.-Abstracts*, Monterey, CA, 2005, p. 198. 05CH37707.

[12] A. L. Peratt, M. A. Van Der Sluijs, and D. A. Scott, "Evidence of an influx of interstellar plasma from archaic Z-pinch recordings," in *Proc. Bull. Amer. Phys. Soc.*, Tampa, FL, Apr. 16–19, 2005. APR05-2005-000897.

[13] M. G. Peratt and A. L. Peratt, "An intense Z-pinch aurora cusp mapped by surveys of recordings from antiquity," in *Proc. IEEE Conf. Rec.-Abstracts*, Traverse City, MI, Jun. 2006, p. 307.

[14] A. H. Qöyawayma and A. L. Peratt, "An intense auroral Z-pinch recorded in antiquity on southwestern artifacts," in *Proc. IEEE Conf. Rec.-Abstracts*, Traverse City, MI, Jun. 2006, p. 318.
[15] A. L. Peratt, J. McGovern, and C. Pedersen, "Intense prehistoric auroral Z-pinch recordings: Surveys of Columbia River Gorge and South Australian petroglyphs," in *Proc. IEEE Conf. Rec.-Abstracts*, Traverse City, MI, Jun. 2006, p. 329.
[16] M. A. Van Der Sluijs and A. L. Peratt, "Intense prehistoric auroral Z-pinch recordings: Surveys South Korean and Thailand petroglyphs," in *Proc. IEEE Conf. Rec.-Abstracts*, Traverse City, MI, Jun. 2006, p. 340.
[17] M. W. Rowe and K. L. Steelman, "Radiocarbon dating of rock paintings using plasma–chemical extraction," *Amer. Lab.*, vol. 34, no. 18, pp. 15–19, Sep. 2002.
[18] K. L. Steelman, M. W. Rowe, V. N. Shirokov, and J. R. Southon, "Radiocarbon dates for pictographs in Ignatievskaya Cave, Russia: Holocene age for supposed Pleistocene fauna," *Antiquity*, vol. 76, no. 292, pp. 341–348, 2002.
[19] K. L. Steelman, M. W. Rowe, and T. W. Boutton, "Stable isotope and radiocarbon analyses of a black deposit associated with pictographs at Little Lost River Cave, Idaho," *J. Archaeol. Sci.*, vol. 29, no. 10, pp. 1189–1198, Oct. 2002.
[20] A. Jensen, R. J. Mallouf, T. Guilderson, K. L. Steelman, and M. W. Rowe, "Radiocarbon assay and X-ray diffraction analysis of pictograph samples from Tall Rockshelter, Davis Mountains, Texas," *J. Big Bend Stud.*, vol. 16, pp. 31–46, 2004.
[21] S. A. Turpin and J. Bass, *The Lewis Canyon Petroglyphs*. San Antonio, TX: Rock Art Found., 1997. Special Publication 2.
[22] G. Mallery, *Picture-Writing of the American Indians*, vol. One and Two. New York: Dover. Reprinted 1972.
[23] J. M. Loring and L. Loring, "Pictographs and petroglyphs of the Oregon country," in *Monograph XXI*. Los Angeles, CA: Inst. Archaeology, Univ. California, 1982.
[24] Z. Chen, *Zhongguo Yanhua Faxian Shi. (History of the Discovery of Chinese Rock Art)*. Shanghai, China: Renmin, 1991.
[25] A. Egeland and W. J. Burke, *Kristian Birkeland, The First Space Scientist*. Dordrecht, The Netherlands: Springer-Verlag, 2005.
[26] A. Brekke and A. Egeland, *The Northern Lights, Their Heritage and Science*. Oslo, Norway, 1994. Grødahl og Dreyers.
[27] S.-I. Akasofu, *Secrets of the Aurora Borealis*. Anchorage, AK: Alaska Geographic, 2002.
[28] C.-G. Fälthammar, "Magnetosphere–ionosphere interactions—Near Earth manifestations of the plasma universe," *IEEE Trans. Plasma Sci.*, vol. PS-14, no. 6, pp. 616–628, Dec. 1986.
[29] J. R. Kan and S.-I. Akasofu, "Electrodynamics of the solar wind–magnetosphere–ionosphere interactions," *IEEE Trans. Plasma Sci.*, vol. 17, no. 2, pp. 83–108, Apr. 1989.
[30] A. J. Dessler, "Solar wind interactions," in *Proc. Birkeland Symp. Aurora and Magn. Storms,* A. Egeland and J. Holtet, Eds., Paris, France: Sur les Presses de L'Imprimerie Tourmon, 1967, pp. 423–430.
[31] U. S. Inan, M. Golkowski, M. K. Casey, R. C. Moore, W. Peter, P. Kulkarni, P. Kossey, and E. Kennedy, "Subionospheric VLF observations of transmitter-induced precipitation of inner radiation belt electrons," *Geophys. Res. Lett.*, vol. 34, no. 2, p. L02106, Jan. 2007.
[32] O. Buneman, T. Neubert, and K.-L. Nishikawa, "Solar wind magnetosphere interaction as simulated by a 3-D, EM particles code," *IEEE Trans. Plasma Sci.*, vol. 20, no. 6, pp. 810–816, Dec. 1992.
[33] A. L. Peratt and C. M. Snell, "Microwave generation from filamentation and vortex formation within magnetically confined electron beams," *Phys. Rev. Lett.*, vol. 54, no. 11, pp. 1167–1170, Mar. 1985.
[34] A. V. Shishlov, R. B. Baksht, A. Y. Labetsky, V. I. Oreshkin, A. G. Rousskikh, A. V. Fedunin, S. A. Chaikovsky, V. A. Kokshenev, N. E. Kurmaev, and F. I Fursov, "Experimental study of an argon-hydrogen Z-pinch plasma radiation source," *IEEE Trans. Plasma Sci.*, vol. 30, no. 2, pp. 498–511, Apr. 2002.
[35] A. Krejci, J. Raus, V. Piffl, A. V. Golubev, Y. Y. Platoov, E. Krousky, and O. Renner, "Multichannel soft X-ray diagnostics of hot plasma evolution in nitrogen-puff Z-pinch," *IEEE Trans. Plasma Sci.*, vol. 21, no. 5, pp. 584–587, Oct. 1993.
[36] H. Alfvén, *Cosmic Plasma*. Dordrecht, The Netherlands: Reidel, 1981.
[37] M. G. Haines, "Dense plasma in Z-pinches and the plasma focus," *Philos. Trans. Roy. Soc. London A, Math. Phys. Sci.*, vol. 300, no. 1456, pp. 649–663, Apr. 1981.
[38] M. M. Milanese and R. L. Moroso, "The first stages of the discharge in a low-energy dense plasma focus," *IEEE Trans. Plasma Sci.*, vol. 33, no. 5, pp. 1658–1661, Oct. 2005.
[39] A. H. Qöyawayma and A. L. Peratt, "The influence of 56 synchrotron radiating Birkeland filaments formed in an archaic auroral sheath on man-made structures and artifacts found worldwide," in *Proc. IEEE Pulsed Power and Plasma Sci. Conf.*, Albuquerque, NM, Jun. 2007, p. 623.
[40] A. L. Peratt, M. A. van der Sluijs, J. McGovern, and P. Bustamante, "Virtual image reconstruction of an intense Z-pinch aurora at Earth's southern axis from archaic petroglyphs," in *Proc. IEEE Pulsed Power and Plasma Sci. Conf.*, Albuquerque, NM, Jun. 2007, p. 623.
[41] W. F. Yao and A. L. Peratt, "Observations of a quadruple from recordings of an intense aurora in prehistory: Three rivers petroglyphs," in *Proc. IEEE Pulsed Power and Plasma Sci. Conf.*, Albuquerque, NM, Jun. 2007, p. 624.
[42] A. B. Kukushkin and V. A. Rantsev-Kartinov, "Self-similarity of plasma networking in a broad range of length scales: From laboratory to cosmic plasmas," *Rev. Sci. Instrum.*, vol. 70, no. 22, pp. 1387–1391, Feb. 1999.
[43] S. Clark, *The Sun Kings*. Princeton, NJ: Princeton Univ. Press, 2007.
[44] V. A. Rantsev-Kartinov, "Observation of the sun self-similarity skeletal structures," in *Proc. Conf. Abstracts, IEEE Int. Conf. Plasma Sci.*, Traverse City, MI, Jun. 2006, p. 269.
[45] C. P. Mountford, "Simple rock engravings in Central Australia," *Man*, vol. 60, pp. 145–147, 1960.

Anthony L. Peratt (S'60–M'63–SM'85–F'99) received the B.S. degree in electrical engineering from California State Polytechnic University, Pomona, in 1963 and the M.S. and Ph.D. degrees in electrical engineering from the University of Southern California, Los Angeles, in 1967 and 1971, respectively.

He was a Staff Member with Lawrence Livermore National Laboratory, in 1972–1979, a Guest Physicist with Max Planck Institut für Plasmaphysik, Garching, Germany, in 1975–1977, a Guest Scientist with Alfvén Laboratory, Royal Institute of Technology, Stockholm, Sweden, in 1985. He was a Scientific Advisor with the United States Department of Energy in 1995–1999. Since 1981, he has been with the Associate Laboratory Directorate for Experimental Programs, Applied Theoretical Physics Division, Physics Division, Los Alamos National Laboratory, Los Alamos, NM. His research interests have included numerical and experimental contributions to high-energy-density plasmas and intense particle beams, inertial-confinement fusion, explosively driven pulsed-power generators, lasers, intense-power-microwave sources, particles, high-energy-density phenomena, new concepts in space propulsion and high-performance computing, plasma cosmogony and cosmology. He is the Author of *Physics of the Plasma Universe* (Springer-Verlag, 1992) and the Editor of *Plasma Astrophysics and Cosmology* (Kluwer Academic Publishers, 1995) and *Advanced Topics in Space and Astrophysical Plasmas* (Kluwer Academic Publishers, 1997).

Dr. Peratt has served as Session Organizer for space plasmas, IEEE International Conference on Plasma Science in 1987–1989, as a Guest Editor of IEEE TRANSACTIONS ON PLASMA SCIENCE, Special Issues on Space Plasmas 1986, 1989, 1990, 1992, 2000, and 2003, as an Organizer of the IEEE International Workshops on Space Plasmas, 1989, 1991, 1993, 1995, 1996, 1997, 1998, and 2003, as an Associate Editor of IEEE TRANSACTIONS ON PLASMA SCIENCE 1989, and as a Senior Editor in 2007. He is an elected member of the IEEE Nuclear and Plasma Science Society (NPSS) Executive Committee (ExCom) in 1987–1989, 1995–1997, and 2004–2007. He has served as a General Chairman of the IEEE International Conference on Plasma Science, Santa Fe, NM, in 1994, as the Vice Chairman of the IEEE NPSS ExCom in 1997, and was elected to the IEEE NPSS Administrative Committee in 1997 and 2004. He is a member of the American Physical Society, American Astronomical Society, and Eta Kappa Nu. He was the recipient of the United States Department of Energy Distinguished Performance Award in 1987 and 1999, the IEEE Distinguished Lecturer Award in 1993, and named the Norwegian Academy of Science and Letters Kristian Birkeland Lecturer in 1995. Dr. Peratt is currently with the Los Alamos National Laboratory Applied Physics Division and also the University of Pennsylvania Museum of Archaeology and Anthropology.

John McGovern completed his schooling in Glasgow, U.K., before immigrating to Australia to undertake explorations in underwater (ocean) archaeology.

He is currently with the Institute for Epigraphic and Aboriginal Recordings, Georgetown, Australia. His research interests include catalog petroglyphs and pictographs according to Aboriginal creation stories. From high energy plasma data, he was able to digitally place together the "shards" of many petroglyphs to gain information about the whole of the instability and its meaning to the people who carved it.

Mr. McGovern is a member of the Adnyamathanha Brotherhood.

Alfred H. Qöyawayma (M'66–LM'06) received the B.S. degree in engineering from California State Polytechnic University, San Luis Obispo, in 1961, the M.S. degree in systems engineering from the University of Southern California, Los Angeles, in 1966, and the Honorary Doctor degree from the University of Colorado, Boulder, in 1986. His graduate works include civil engineering and hydrology and power systems engineering.

He trained initially as a toolmaker prior to academic pursuit. In 1961, he became a member of the technical staff with the Research Division, Litton Guidance and Control Systems, Woodland Hills, CA. From 1961 to 1971, he was involved in research and development, mathematical simulation and prototype development of Inertial Measurement Units (IMU) and star trackers for a missile guidance course correction system. He is the holder of U.S. and International patents for a new IMU design, Scientific American, in 1969. Applications of his work included X-15 and several military and commercial applications (F-15, Boeing 747). He participated in the development of long-range optical tracking systems and the first aircraft laser-range-finder/target-designation system. From 1971 to 1990, he became the Manager and formed the environmental research and planning group at the Salt River Project, an electric and water utility in Phoenix, AZ. He directed the policy development and environmental research for the location and licensing of large power plants, transmissions, and railroads. His researches are in the long-range transport of pollutants, visibility, health effects of electromagnetic fields, global CO_2, and ecological impacts. His water projects included the system reconfiguration of the Central Arizona Project to the presently implemented "Plan 6." He was integrally involved in the management team reviewing scientific research projects of the Electric Power Research Institute throughout the United States. In 1990, he became an Independent Researcher and Ceramic Artist (alqpottery.com) exhibiting and lecturing through the U.S., with a focus on the peopling of the Americas through epigraphic research. As part of his independent research, he has engaged in archaeological studies in Mexico, Honduras, and Peru. His current research involves in the identification of artifacts from antiquity and prehistory epigraphy to high-energy space plasma physics phenomena. His ceramic work has been flown on the International Space Station and is currently on exhibit at Smithsonian's National Museum of the American Indian (NMAI). He is the cofounder and founding Chairman of the American Indian Science and Engineering Society, working with the National Academy of Engineering and Science, in 1978. In 1988, he has a joint research with the Smithsonian Conservation Analytical Laboratory that was published in the Journal of Field Archaeology (vol. 15, no. 3, pp. 317–337, 1988): "The Formation of Ceramic Analytical Groups: Hopi Pottery Production and Exchange, AD 1300–1600. In 1988, he received a Presidential Appointment under Public Law 99-498 and served six years as the Vice Chairman of the Institute of American Indian Art, Santa Fe, NM. He is currently a Consultant with NMAI and the Museum of Natural History and founder of Qöyawayma Ceramics and Epigraphics.

Dr. Qöyawayma became a Fulbright Fellow in his work with the Polynesian Maori of New Zealand. He is a member of the Hopi Tribe, Arizona.

Marinus Anthony Van der Sluijs was born in Rotterdam, The Netherlands. He received the M.A. degree in comparative and historical linguistics, specializing in the Indo–European and Semitic language families, from Leiden University Centre for Linguistics, Leiden, The Netherlands, in 1999.

He has devoted his time to the study of archaeoastronomy, ancient cosmologies, and the history of astronomy. He is currently with Mythopedia, London, U.K. He has researched and interviewed the Maya people in Belize and Guatemala and the Sundanese on Java. He has GPS-logged petroglyphs in Valcamonica, Italy; Mongolia; South Korea; Thailand; Hawaii; Ireland; and the United Kingdom. While he has published a number of articles on these subjects in relevant academic journals, he is currently preparing a comprehensive textbook of worldwide traditions concerning the axis mundi or "universal axis" and its possible origins in historical disturbances of the Earth's plasmasphere. He is fluent in English, German, Dutch, French, Italian, Spanish, and beginners' Korean. His research involves in-depth studies of Latin, Greek, Hebrew, Aramaic, Gothic, Sanskrit, Hittite, Hurrian, Assyro–Babylonian, and Sumerian.

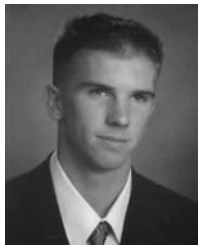

Mathias G. Peratt (S'03–M'06) received the B.S. and M.S. degrees in electrical engineering from the University of Southern California (USC), Los Angeles, in 2004 and 2007, respectively.

He was with USC Schools of Cinema-Television and Multimedia-Technology in 1999–2006. He was an Engineer with Space Airborne Division, Raytheon Corporation, El Segundo, California, in 2004–2006, and is currently an Engineer with the Network Communications Systems, Raytheon Corporation, Fullerton, California. He is a high-altitude difficult-terrain GPS petroglyph logger of Los Alamos, New Mexico, and Arizona research teams. He is a multimedia analyst of world petroglyph data.